DEVELOPMENT OF NON-NOBLE ELECTROCATALYSTS FOR QUINONE BASED ORGANIC REDOX FLOW BATTERIES

Submitted in partial fulfillment of the requirement for the award of the degree of

DOCTOR OF PHILOSOPHY

in

CHEMICAL ENGINEERING

by

IRSHAD ULLAH KHAN

Roll No: 719137

Under the supervision of

Dr. MURALI MOHAN SEEPANA

Associate Professor

(Supervisor)

Dr. K.S. RAJMOHAN

Assistant Professor

(Co-Supervisor)

DEPARTMENT OF CHEMICAL ENGINEERING

NATIONAL INSTITUTE OF TECHNOLOGY WARANGAL

TELANGANA – 506004, INDIA.

November 2023

NATIONAL INSTITUTE OF TECHNOLOGY

Warangal – 506004, Telangana, INDIA.

CERTIFICATE

This is to certify that the thesis entitled "Development of Non-Noble Electrocatalysts for Quinone Based Organic Redox Flow Batteries" being submitted by **Mr. Irshad** for the award of the degree of Doctor of Philosophy (Ph.D) in Chemical Engineering, National Institute of Technology, Warangal, India, is a record of the bonafide research work carried out by him under my supervision. The thesis has fulfilled the requirements according to the regulations of this Institute and in my opinion, has reached the standards for submission. The results embodied in the thesis have not been submitted to any other University or Institute for the award of any degree or diploma.

Dr. K.S. Rajmohan
Thesis Co-Supervisor
Assistant Professor
Department of Chemical Engineering

Dr. Murali Mohan Seepana
Thesis Supervisor
Associate Professor
Department of Chemical Engineering

Date: 10-11-2023
National Institute of Technology, Warangal, India.

This thesis is dedicated to

MY FAMILY

for their endless love,

support and encouragement.

DECLARATION

This is to certify that the work presented in the thesis entitled "**Development of Non-Noble Electrocatalysts for Quinone Based Organic Redox Flow Batteries**" is a bonafide work done by me under the supervision of Dr. Murali Mohan Seepana and Dr. K.S. Rajmohan and is not submitted elsewhere for the award of any degree.

I declare that this written submission represents my ideas in my own words and where other's ideas or words have been included, I have adequately cited and referenced the original source. I also declare that I have adhered to all principles of academic honesty and integrity and have not misrepresented or fabricated or falsified any idea/data/fact/source in my submission.

I understand that any violation of the above will be a cause for disciplinary action by the Institute and can also evoke penal action from the sources which have thus not been properly cited or from whom proper permission has not been taken when needed.

IRSHAD
Roll No.719137

ACKNOWLEDGMENTS

It gives me immense pleasure to express my heartiest and sincere gratitude, indebtedness to my supervisor **Dr. Murali Mohan Seepana** for his patient guidance, timely appreciation, extraordinary support, enormous enlightening discussion with constructive criticism, and sustain inputs during the research work and preparation of the thesis. I would like to thank my co-supervisor **Dr. K.S. Rajmohan** for his valuable insights and constant support throughout the research journey.

I am very much thankful to **Dr. P.V. Suresh**, Head of the Department of Chemical Engineering for their advice and encouragement. I take this privilege to thank all my Doctoral Committee members, **Prof. A. Sarath Babu,** Professor**,** Department of Chemical Engineering, **Prof. K.V. Gobi**, Professor, Department of Chemistry and **Dr. Anjana P.A.**, Assistant Professor, Department of Chemical Engineering for their detailed review, constructive suggestions and excellent advice during the progress of this research work. I also appreciate the encouragement from teaching, non-teaching members, fellow scholars and the fraternity of the Department of Chemical Engineering of NIT Warangal. They have always been encouraging and supportive.

I wish to express my sincere thanks to **Prof. Bidyadhar Subudhi**, Director, NIT Warangal for his official support and encouragement. There is no way to express how much it meant to me to have been a research scholar in NIT Warangal.

I would like to express my deepest gratitude to my parents **Mr. Ahmed Ullah Khan**, **Mrs. Sharifunnisa Khan** and my brother **Mr. Ashfak Ullah Khan**. Their love and support have been the foundation upon which I've built my academic and personal achievements. I am forever grateful for your endless love and encouragement.

I want to extend my heartfelt appreciation to my beloved wife **Mrs. Zeba Khan**, for her patience, understanding, and constant encouragement throughout my research journey. This thesis is a testament to the partnership and love that we share. It would not have been possible without your unwavering belief in me and our dreams together.

Irshad U. Khan

ABSTRACT

The surge in global energy generation from renewable sources has triggered the need for large-scale electrical energy storage technologies. These storage technologies act like a bridge between generation and end usage. Recently, the vanadium redox flow battery (VRFB) technology has taken the lead in the market; however, the high cost of vanadium electrolyte raises concern over commercial usage. In this work, the organic flow battery systems have been proposed as an alternative to VRFB as they are simple, economical, and abundantly available. The quinone-based redox chemistry was explored and proposed two battery systems, i.e., (i) hydrogen-1,4 p-Benzoquinone redox flow battery (H_2-BQ RFB) and (ii) hydroquinone-benzoquinone redox flow battery (HQ-BQ RFB). Carbon-based electrodes are extensively used as electrode materials due to their comprehensive properties, but they possess poor hydrophilic nature and low electrochemical activity. It is essential to modify carbon-based materials before employing them in battery applications. Numerous techniques are proposed to refine carbon-based materials. The modification by incorporating catalysts is one of the best ways to improve redox kinetics. Metal oxides are widely preferred as electrocatalysts to modify carbon due to their low cost, tunability, and high activity. The Tungsten trioxide (WO_3) and Titanium dioxide (TiO_2) have already proved their suitability in energy systems with exceptional electrochemical activity. Hence, these materials are proposed for the first time for the H_2-BQ RFB and HQ-BQ RFB.

The present work focuses on developing non-noble Tungsten trioxide-doped carbon (WO_3/C) and TiO_2 supported on carbon nanoparticles (TiO_2@CNP) electrocatalyst for proposed organic redox flow batteries. The catalysts are characterized by field emission scanning electron microscope (FESEM) for topography, X-ray diffraction (XRD) for examining crystallinity, and Fourier transform infrared spectroscopy (FTIR) for identifying the functional bonds. TiO_2@CNP and WO_3/C electrocatalysts are tested in positive half-cell of H_2-BQ RFB and single-cell HQ-BQ RFB, respectively. The electrochemical activity of the electrocatalysts is evaluated by cyclic voltammetry (CV). The voltammograms of TiO_2@CNP-CP in positive half-cell of H_2-BQ RFB, TiO_2@CNP-CP in both half cells of HQ-BQ RFB and WO_3/C of in both half cells of HQ-BQ RFB were recorded. These show high anodic and cathodic peak currents, low charge transfer resistance, and relatively high electro-kinetic reversibility. Enhanced electrochemical active surface area (ECSA) and turnover frequency (TOF) revealed higher electrode kinetics than the pristine carbon paper. ECSA of WO_3/C-CP and TiO_2@CNP-CP in

positive half-cell of HQ-BQ RFB are 10 cm^2 and 8.33 cm^2 respectively while in negative half-cell of HQ-BQ RFB are 4.8 cm^2 and 2.25 cm^2. The higher ECSA implies that the WO_3/C-CP provides more active sites for the reactions to take place in the battery system. The calculated number of active sites of WO_3/C-CP in the positive half-cell and the negative half-cell of HQ-BQ RFB are 4.3×10^{-6} mol and 2.6×10^{-6} mol, respectively. The corresponding TOF of WO_3/C-CP in the positive and negative half-cells of HQ-BQ RFB are 0.19 s^{-1} and 0.079 $s^{-1,}$ respectively. These values are observed to be higher than that of CP, TiO_2@CNP-CP, and possess improved catalytic activity. The TiO_2@CNP electrocatalyst was tested in an H_2-BQ RFB positive half-cell by galvanostatic charge-discharge and obtained energy efficiency of up to 73%. The charge–discharge test on single cell HQ-BQ RFB was conducted using pristine carbon paper (CP), TiO_2@CNP-CP, and WO_3/C coated carbon paper (WO_3/C-CP). The columbic efficiency (CE), voltage efficiency (VE), and energy efficiency (EE) of the RFB using WO_3/C-CP are around 90%, 75%, and 70%, respectively, which are significantly higher than the CP and TiO_2@CNP-CP. The developed non-noble WO_3/C and TiO_2@CNP electrocatalysts proved their suitability in proposed H_2-BQ RFB and HQ-BQ RFB systems by providing higher active sites and reaction kinetics.

TABLE OF CONTENTS

List of Tables

List of Figures

List of Symbols

E°	Standard theoretical potential (V)
a	Tafel intercept (V)
b	Slope of the linear fit Tafel plot (mV)
j	Current density (mA cm^{-1})
H^{+}	Proton
e^{-}	Electron
η	Overpotential (V)
V	Potential (V)
I	Current (A)
Ipa	Anodic peak current (A)
Ipc	Cathodic peak current (A)
C_{dl}	Double layer capacitance (F)
Cs	Specific capacitance (F cm^{-2})
ν	Scan rate (mV/s)
F	Faraday's constant (coulomb/mol),
n	Number of active sites (mol).

List of Abbreviations

EES	Electrical Energy Storage
EEES	Electrochemical Electrical Energy Storage
LIB	Li-Ion battery
LAB	Lead-Acid Battery
RFB	Redox Flow Battery
VRFB	Vanadium RFB
DoE	Department of Energy
ORFB	Organic RFB
TEMPO	2,2,6,6- tetramethylpiperidin-1-yl)oxyl
ARFB	Aqueous RFB
Pt	Platinum
Zn-Br RFB	Zinc-Bromine RFB
Fe-Cr RFB	Iron-Chromium RFB
NASA	National Aeronautics and Space Administration
SPEEK	Sulfonated Poly(Ether Ether Ketone)
BQDS	4,5-Dihydroxybenzene-1,3- Disulfonic Acid

AQDS	Anthraquinone-2,6-Disulfonic Acid
TiO_2@CNP	Carbon Nanoparticles Supported Titanium Dioxide
WO_3/C	Carbon Nanoparticles Supported Tungsten Dioxide
TiO_2@CNP-CP	TiO_2@CNP Coated Carbon Paper
WO_3/C-CP	WO_3/C Coated Carbon Paper
AEM	Anion Exchange Membrane
CEM	Cation Exchange Membrane
PES	Poly(Ether Sulfone)
TiO_2	Titanium Dioxide
WO_3	Tungsten Trioxides
FESEM	Field Emission Scanning Electron Microscope
EDX	Energy Dispersive X-Ray
FTIR	Fourier Transform Infrared Spectroscopy
XRD	X-ray Diffraction
CV	Cyclic Voltammetry
GCD	Galvanostatic Charge-Discharge
BQ	Benzoquinone

HQ	Hydroquinone
IPA	Isopropanol
CNP	Carbon Nanoparticles
CP	Carbon Paper
PGSTAT	Potentiostat/Galvanostat System
WO_3/C-GC	WO_3 coated Glassy Carbon Electrode
ECSA	Electrochemical Active Surface Area (cm^2/g)
TOF	Turnover Frequency (s^{-1})
CE	Columbic Efficiency (%)
VE	Voltage Efficiency (%)
EE	Energy Efficiency (%)

CHAPTER 1

INTRODUCTION

Chapter 1

Introduction

Electricity is a basic need of humans globally, and a significant part of the electrical energy has been generated from fossil fuels. These sources are limited and raise concerns about the environment. Hence, a rapid shift is observed from fossil to renewable sources. Renewable energy generation technologies are well-developed and produce 30% of global electricity demand (Bocca et al., 2023). It is essential to employ 'Electrical Energy Storage' (EES) for maximum utilization of the excess electricity generated from fossil fuels and renewable energy sources together.

1.1 EES

The Electrical Energy Storage (EES) technologies serves as a bridge between generation and end usage, facilitating efficient management and utilization of electricity. As depicted in Figure 1.1 (Guney & Tepe, 2017) various EES technologies play crucial roles in this ecosystem.

Among these technologies, Pumped Storage Hydropower (PSH) and Compressed Air Energy Storage (CAES) exhibit remarkable power ratings, boasting capacities of up to 1GW. However, these technologies encounter limitations stemming from geographical and hydrological constraints (Lindley, 2010).

Electrochemical Electrical Energy Storage (EEES) technologies, on the other hand, offer a plethora of advantages, including heightened energy and power density, scalability, rapid response times, and geographical versatility (He et al., 2021). EEES technologies encompass several subcategories such as supercapacitors, solid-state batteries, liquid-state batteries, and flow batteries (Arote, 2021). These technologies, distinguished by their rated power, find applications across industrial, residential, and transportation sectors. Lithium-ion batteries (LIBs), renowned for their high energy density, primarily cater to the demand for portable electronics and automotive applications. However, their widespread adoption is impeded by factors such as high costs and safety concerns (Shahid & Agelin-Chaab, 2022). In contrast, Lead-acid batteries (LABs) are extensively utilized in residential settings due to their affordability and safe operational characteristics at low prices. Nonetheless, LABs suffer from drawbacks such as short lifespans, low energy densities, and environmental ramifications associated with the disposal of used lead electrolytes (Roy et al., 2022).

Advancements in flow battery systems have led to improved power ratings through a unique approach involving the partial separation of energy storage (external tanks) and power generation (battery cell), as illustrated in Figure 1.1. Notably, Redox Flow Battery (RFB) technology emerges as a promising alternative, offering a versatile, durable, and secure solution for large-scale stationary energy storage needs. With their distinct characteristics and capabilities, EEES technologies collectively contribute to enhancing the efficiency and resilience of modern energy systems, addressing the evolving demands of diverse applications.

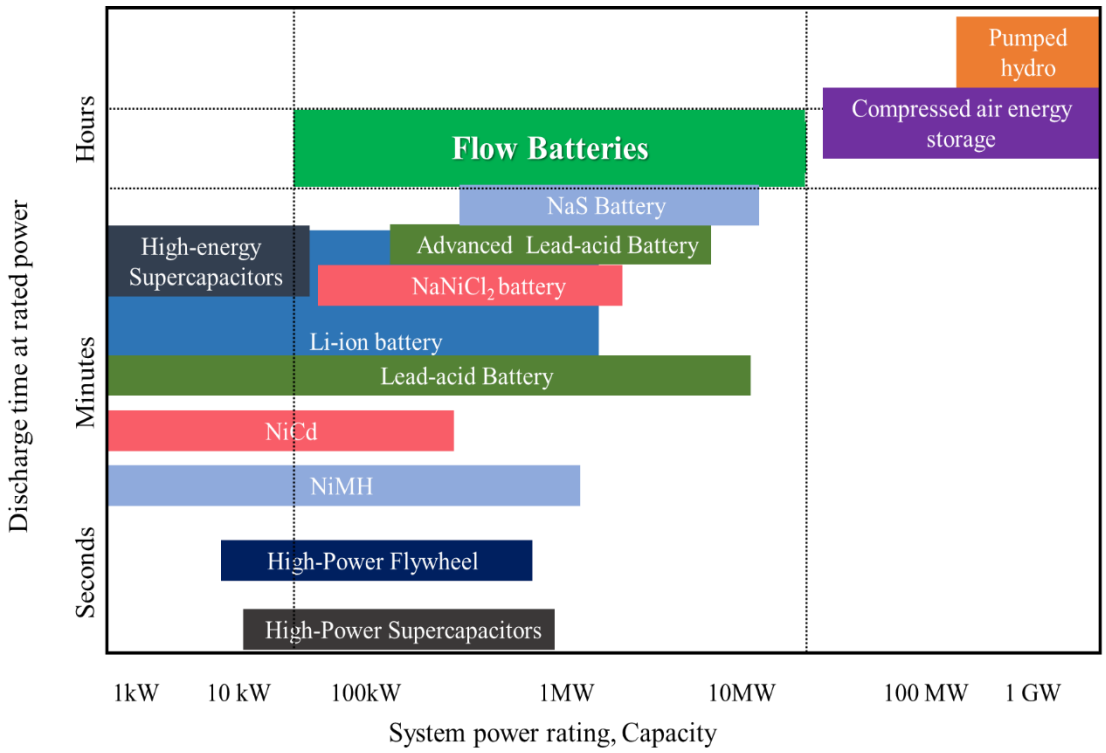

Figure 1.1. Comparison of ESSs based on the power ratings and discharge time (Guney & Tepe, 2017)

1.2 Flow battery system

Redox flow batteries have garnered significant attention in the pursuit of scalable and versatile energy storage solutions, primarily due to their ability to address the intermittent nature of renewable energy sources. This technology offers various advantages, including an extended operational lifespan, heightened safety features, the capability to undergo deep charge-discharge cycles, and a cost-effective design.

A single-cell redox flow battery comprises porous electrodes, a membrane, bipolar plates, current collectors, and external electrolyte storage tanks, as depicted in Figure 1.2. Throughout the operational cycle, the anolyte and catholyte are pumped into their respective chambers within the cell. During the discharge phase, the negative electrode undergoes the oxidation of active material, resulting in the loss of electrons. Conversely, at the positive electrode, reduction

takes place, leading to electron gain. During the charge cycle, the reverse reaction kinetics occur.

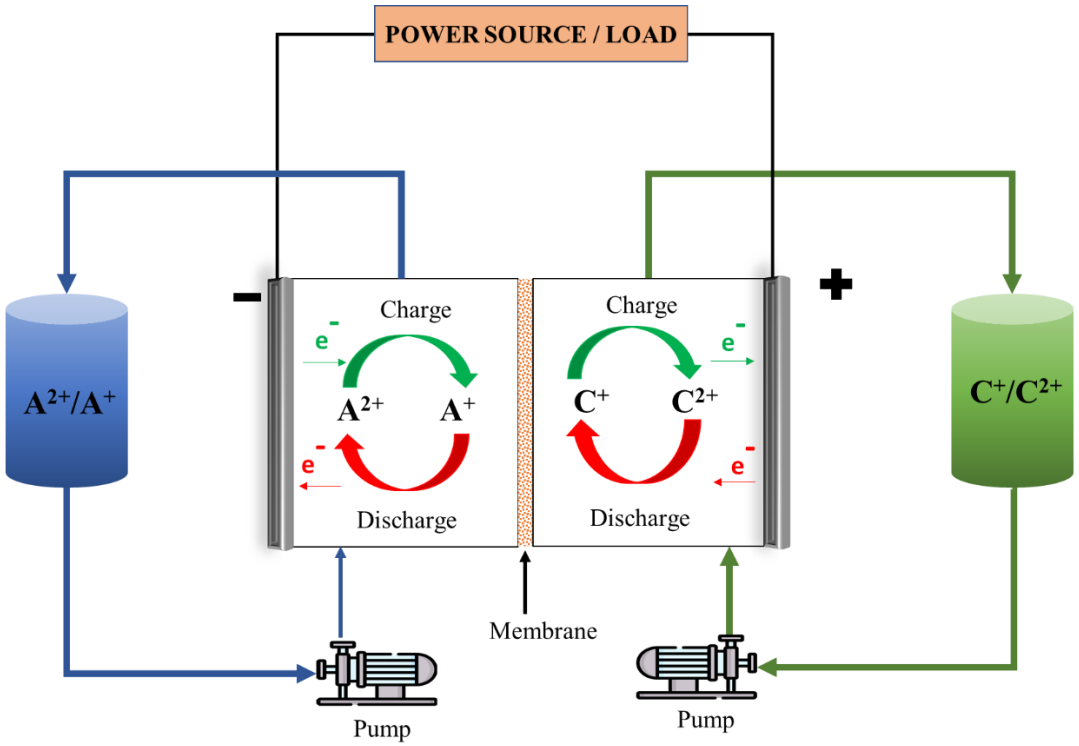

Figure 1.2 Working mechanism of Redox Flow Battery

$$A^{2+} + C^{+} \underset{\text{discharge}}{\overset{\text{charge}}{\rightleftharpoons}} A^{+} + C^{2+} \qquad (1.1)$$

The transfer of ions across the membrane is crucial for maintaining charge neutrality, facilitating the continuous flow of electricity during both charging and discharging processes. This intricate interplay of electrochemical processes underscores the efficiency and functionality of redox flow batteries in the dynamic landscape of energy storage technologies. Flow batteries are classified based on the redox couples they employ, and several prominent chemistries have emerged in recent research. Noteworthy among these are iron/chromium RFBs (LI, 2021),, zinc/bromide RFBs (Naresh et al., 2022), zinc/iron (M. Yang et al., 2022),

vanadium RFBs (VRFBs) (Huang et al., 2023), and organic RFBs. Among these, the VRFB stands out as a cutting-edge battery technology that utilizes vanadium ions at four oxidation states in both half-cells, effectively eliminating cross-mixing issues. Despite being a matured technology and currently dominating the market due to its high cell potential (1.5V), superior energy efficiency, and prolonged lifespan, challenges persist. These include the high costs associated with vanadium, expensive membranes, elevated corrosion rates, and the precipitation of V2O5 at temperatures exceeding 45 ℃ (Kim & Jeon, 2017). To meet the Department of Energy's (DoE) target cost of $150/kWh for flow batteries, exploration into alternative flow redox chemistries becomes imperative (Emmett & Roberts, 2021) Identifying chemistries with higher redox potential, robust stability, and improved economic viability is crucial to addressing the limitations faced by current technologies and advancing the broader adoption of flow batteries in the evolving landscape of energy storage.

1.3 Need for Organic Redox Flow Batteries (ORFB)

Organic redox couples possess long-term stability, abundant availability, low cost, and good variable redox potentials. Hence, this flow chemistry is explored as a potential solution to replace the vanadium active material in achieving the targeted cost of RFB. These redox couples significantly control the redox potential and solubility in supporting electrolytes. This control is achieved by incorporating specific functional groups into the organic molecule's structure, resulting in affordable and high-energy-density ORFBs (Diaz-Muñoz et al., 2018). Sometimes, even a single organic redox couple can serve in both the anolyte and catholyte, eliminating physical crossover and enhancing. The investigation of well-known organic active materials such as quinones, viologens, alloxazine, and 2,2,6,6- tetramethylpiperidin-1-yl)oxyl (TEMPO) for ORFBs is emerging (Lin et al., 2015). The quinones and their derivatives exhibit considerable promise as prospective alternatives due to their advantageous characteristics, notably low toxicity, cost-efficiency, and robust reaction reversibility (Silverstein & Rose,

2022). Quinones, readily occurring in nature and pivotal in processes such as photosynthesis, though possessing equilibrium potentials that are relatively modest for battery applications, offer an intriguing avenue for enhancement.

1.4 Challenges in quinone-based RFB

QRFBs have the following limitations, which need to be addressed

i. Quinone solubility in the supporting electrolyte (Hofmann & Schröder, 2019).
ii. Membrane selectivity, conductivity, and durability (Yuan et al., 2022).
iii. Sluggish reaction kinetics (Z. Yang et al., 2018b).

Currently, researchers are working intensely to overcome the mentioned challenges. An increase in quinone solubility in the supporting electrolyte was observed by increasing the pH (Ding & Yu, 2016), substitution of a proton with Na^+ ions in the quinone ring (Y. Yang et al., 2023), and introduction of the sulfonic acid group on quinone molecules (Hoober-Burkhardt et al., 2017). Maintaining electrolyte equilibrium is crucial when using a high-performance separator. The ideal membranes for RFB must balance selectivity, conductivity, and durability (Arora & Zhang, 2004). Nafion membranes are widely used for all RFBs, including QRFBs (Nasser et al., 2018; Yu et al., 2019). SPEEK membranes have improved performance in quinone-based ORFBs (Pinheiro et al., 2023). Sluggish reaction kinetics of the liquid electro-active material in aqueous redox flow battery (ARFB) chemistries can be improved by modifying the electrode, heat treatment, chemical treatment, and using the electrocatalyst (González et al., 2012; Jiang et al., 2019). The introduction of an electrocatalyst to the electrodes improves the kinetics of redox reactions and enables an increase in power density. Nd_2O_3 and Pt-modified carbon electrodes exhibited higher energy efficiency and high discharge capacities for VRFBs (Fetyan et al., 2018; Jeong et al., 2013). Platinum (Pt) was applied to the surface of glass fibers (GFs) and subjected to heat treatment, which improved the kinetics of the Zn-Br_2 RFB (Mariyappan et al., 2021). A sandwiched electrode featuring skeletal Cu_7S_4

nanocages on a graphite-felt substrate was employed to enhance the performance of polysulfide-iodide RFB (Zai et al., 2020). The deposition of metal (Ir, Bi, Cu) and metal oxide (ZrO_2, CrO_2) on carbon-based electrodes has shown enhanced reaction kinetics (Gautam et al., 2020) in RFB operations.

1.5 Motivation for the development of an electrocatalyst for quinone-based RFB

Aqueous quinone-based Redox Flow Batteries (RFBs) are characterized by sluggish electrode kinetics (Z. Yang et al., 2018a). In these systems, carbon felt/carbon paper is commonly employed directly as electrodes, resulting in an energy efficiency limitation of up to 58% (Jin et al., 2019). Interestingly, existing literature does not provide insights into the utilization of electrocatalyst materials to ameliorate the energy efficiency of quinone-based RFBs.

Addressing this research gap, the current study endeavors to pioneer advancements by developing non-precious metal catalysts specifically designed for enhancing the efficiency of quinone-based RFBs. This novel approach involves the exploration of non-precious metal oxide-based electrocatalysts, namely TiO_2@CNP and WO_3/C, tailored for application in H_2-BQ RFB and HQ-BQ RFB systems. Through systematic testing, these electrocatalysts evaluated for their efficacy in augmenting the overall performance and energy efficiency of quinone-based RFBs, paving the way for more sustainable and efficient energy storage solutions.

1.6 Thesis layout

The thesis is organized into six chapters, including the current part as Chapter 1, which briefly introduces EES and flow Battery systems. It also illustrates the need for organic redox flow batteries, challenges, and motivation for developing electrocatalysts.

Chapter 2 provides a detailed literature review on electrocatalysts for redox flow batteries (RFBs), especially on Quinone-based RFBs. It contains types of RFBs, components, the

working principle of Quinone-based RFB, and the role of each component in boosting the cell's performance. The research gaps and the objectives of the thesis work are also presented.

Chapter 3 gives deep insight into the experimental studies, synthesis, and characterization of TiO_2@CNP and WO_3/C electrocatalysts. The detailed characterization procedures of electrocatalysts and the testing of single cells in H_2-BQ and HQ-BQ RFBs are explained.

Chapter 4 provides a detailed analysis of results related to the physicochemical and electrochemical characterization of TiO_2@CNP electrocatalyst and its suitability in the positive half-cell of H_2-BQ RFB.

Chapter 5 provides detailed discussions of the synthesis and characterization results of the WO_3/C electrocatalyst. The results related to the physicochemical and electrochemical characterization of WO_3/C electrocatalyst and its suitability in both half-cells of HQ-BQ RFB. This chapter also presents an in-depth analysis of the performance of HQ-BQ RFB with WO_3/C and previously developed TiO_2@CNP.

Chapter 6 provides the overall conclusion drawn from the present work, along with the scope for future work.

References

Arora, P., & Zhang, Z. (2004). Battery separators. Chemical Reviews, 104(10), 4419–4462. https://doi.org/10.1021/cr020738u

Arote, S. A. (2021). Electrochemical energy storage mechanisms and performance assessments: an overview. In Electrochemical Energy Storage Devices and Supercapacitors (pp. 1–34). https://doi.org/10.1088/978-0-7503-3103-6ch1

Bocca, R., Ashraf, M., & Jamison, S. (2023). Fostering Effective Energy Transition 2023 Edition. World Economic Forum, April, 1–52. https://www3.weforum.org/docs/WEF_Fostering_Effective_Energy_Transition_2023.pdf

Diaz-Muñoz, G., Miranda, I. L., Sartori, S. K., de Rezende, D. C., & Diaz, M. A. N. (2018). Chapter 11 - Anthraquinones: An Overview (B. T.-S. in N. P. C. Atta-ur-Rahman (ed.); Vol. 58, pp. 313–338). https://doi.org/10.1016/B978-0-444-64056-7.00011-8

Ding, Y., & Yu, G. (2016). A Bio-Inspired, Heavy-Metal-Free, Dual-Electrolyte Liquid Battery towards Sustainable Energy Storage. Angewandte Chemie - International Edition. https://doi.org/10.1002/anie.201600705

Fetyan, A., El-Nagar, G. A., Derr, I., Kubella, P., Dau, H., & Roth, C. (2018). A neodymium oxide nanoparticle-doped carbon felt as promising electrode for vanadium redox flow batteries. Electrochimica Acta, 268, 59–65. https://doi.org/10.1016/j.electacta.2018.02.104

Gautam, R. K., Kapoor, M., & Verma, A. (2020). Tactical Surface Modification of a 3D Graphite Felt as an Electrode of Vanadium Redox Flow Batteries with Enhanced Electrolyte Utilization and Fast Reaction Kinetics. Energy and Fuels, 34(4), 5060–5071. https://doi.org/10.1021/acs.energyfuels.0c00701

González, Z., Botas, C., Álvarez, P., Roldán, S., Blanco, C., Santamaría, R., Granda, M., & Menéndez, R. (2012). Thermally reduced graphite oxide as positive electrode in Vanadium Redox Flow Batteries. Carbon, 50(3), 828–834. https://doi.org/10.1016/j.carbon.2011.09.041

Guney, M. S., & Tepe, Y. (2017). Classification and assessment of energy storage systems. Renewable and Sustainable Energy Reviews, 75, 1187–1197. https://doi.org/10.1016/j.rser.2016.11.102

He, W., King, M., Luo, X., Dooner, M., Li, D., & Wang, J. (2021). Technologies and economics of electric energy storages in power systems: Review and perspective. Advances in Applied Energy, 4, 100060. https://doi.org/10.1016/j.adapen.2021.100060

Hofmann, J. D., & Schröder, D. (2019). Which Parameter is Governing for Aqueous Redox Flow Batteries with Organic Active Material? Chemie-Ingenieur-Technik, 91(6), 786–794. https://doi.org/10.1002/cite.201800162

Hoober-Burkhardt, L., Krishnamoorthy, S., Yang, B., Murali, A., Nirmalchandar, A., Prakash, G. K. S., & Narayanan, S. R. (2017). A New Michael-Reaction-Resistant Benzoquinone for Aqueous Organic Redox Flow Batteries. Journal of The Electrochemical Society.

https://doi.org/10.1149/2.0351704jes

Huang, Z., Liu, Y., Xie, X., Huang, Q., & Huang, C. (2023). Experimental study on efficiency improvement methods of vanadium redox flow battery for large-scale energy storage. Electrochimica Acta, 466, 143025.
https://doi.org/10.1016/j.electacta.2023.143025

Jeong, S., Kim, S., & Kwon, Y. (2013). Performance enhancement in vanadium redox flow battery using platinum-based electrocatalyst synthesized by polyol process. Electrochimica Acta, 114, 439–447.
https://doi.org/10.1016/j.electacta.2013.10.011

Jiang, Y., Cheng, G., He, Z., Chen, J., Li, Y., Zhu, J., Meng, W., Zhou, H., Dai, L., & Wang, L. (2019). Biomass-Derived Porous Graphitic Carbon with Excellent Electrocatalytic Performances for Vanadium Redox Reactions. Journal of The Electrochemical Society, 166(16), A3918.
https://doi.org/10.1149/2.0941915jes

Jin, S., Jing, Y., Kwabi, D. G., Ji, Y., Tong, L., De Porcellinis, D., Goulet, M.-A., Pollack, D. A., Gordon, R. G., & Aziz, M. J. (2019). A Water-Miscible Quinone Flow Battery with High Volumetric Capacity and Energy Density. ACS Energy Letters, 4(6), 1342–1348. https://doi.org/10.1021/acsenergylett.9b00739

Kim, D., & Jeon, J. (2017). A high-temperature tolerance solution for positive electrolyte of vanadium redox flow batteries. Journal of Electroanalytical Chemistry, 801, 92–97. https://doi.org/10.1016/j.jelechem.2017.07.037

LI, L. (2021). A 250 kWh Long-Duration Advanced Iron-Chromium Redox Flow Battery. ECS Meeting Abstracts, MA2021-01(3), 222.
https://doi.org/10.1149/MA2021-013222mtgabs

Lin, K., Chen, Q., Gerhardt, M. R., Tong, L., Kim, S. B., Eisenach, L., Valle, A. W., Hardee, D., Gordon, R. G., Aziz, M. J., & Marshak, M. P. (2015). Alkaline quinone flow battery. Science.
https://doi.org/10.1126/science.aab3033

Lindley, D. (2010). Smart grids: The energy storage problem. Nature, 463(7277), 18–20. https://doi.org/10.1038/463018a

Mariyappan, K., Ragupathy, P., & Ulaganathan, M. (2021). Enhancement of Bromine Kinetics Using Pt@Graphite Felt and Its Applications in Zn-Br2 Redox Flow Battery. Journal of The Electrochemical Society, 168(9), 90566.
https://doi.org/10.1149/1945-7111/ac2707

Naresh, R. pandiyan, Surendran, A., Ragupathy, P., & Dixon, D. (2022). Enhanced electrochemical performance of zinc/bromine redox flow battery with carbon-nanostructured felt generated by cobalt ions. Journal of Energy Storage, 52, 104913. https://doi.org/10.1016/j.est.2022.104913

Nasser, R., Hubadillah, S. K., Othman, M. H. D., & Mohamed Hassan, A. A. (2018). Fabrication and Characterization of Low-Cost Poly(Vinyl Alcohol) Composite Membrane for Low Temperature Fuel Cell Application. Journal of Applied Membrane Science & Technology, 22(1), 55–63.

https://doi.org/10.11113/amst.v22n1.128

Pinheiro, D., Sousa, J. F. M., Pineiro, M., Valente, A. J. M., & Seixas de Melo, J. S. (2023). Non-pre-treated sulfonated poly(ether ether ketone) membrane as an efficient alternative for Nafion in acidic aqueous organic redox flow batteries. Journal of Energy Storage, 57, 106201. https://doi.org/10.1016/j.est.2022.106201

Roy, A., Patil, R. B., & Sen, R. (2022). The effect of fast charging and equalization on the reliability and cycle life of the lead acid batteries. Journal of Energy Storage, 55, 105841. https://doi.org/10.1016/j.est.2022.105841

Shahid, S., & Agelin-Chaab, M. (2022). A review of thermal runaway prevention and mitigation strategies for lithium-ion batteries. Energy Conversion and Management: X, 16, 100310.
https://doi.org/10.1016/j.ecmx.2022.100310

Silverstein, T. P., & Rose, J. R. (2022). Dependence of Quinone Electrochemistry on Solvent Polarity and pH. JOURNAL OF THE ELECTROCHEMICAL SOCIETY, 169(4). https://doi.org/10.1149/1945-7111/ac5efe

Singh, V., Kim, S., Kang, J., & Byon, H. R. (2019). Aqueous organic redox flow batteries. Nano Research, 12(9), 1988–2001.
https://doi.org/10.1007/s12274-019-2355-2

Yang, M., Xu, Z., Xiang, W., Xu, H., Ding, M., Li, L., Tang, A., Gao, R., Zhou, G., & Jia, C. (2022). High performance and long cycle life neutral zinc-iron flow batteries enabled by zinc-bromide complexation. *Energy Storage Materials*, *44*, 433–440. https://doi.org/10.1016/j.ensm.2021.10.043

Yang, Y., Wang, D., Zheng, J., Qin, X., Fang, D., Wu, Y., & Jing, M. (2023). Interionic hydrogen bonds induced high solubility of quinone derivatives and preliminary study on their application properties in all quinone aqueous redox flow battery. Electrochimica Acta, 452, 142292.
https://doi.org/10.1016/j.electacta.2023.142292

Yang, Z., Tong, L., Tabor, D. P., Beh, E. S., Goulet, M.-A., De Porcellinis, D., Aspuru-Guzik, A., Gordon, R. G., & Aziz, M. J. (2018a). Flow Batteries: Alkaline Benzoquinone Aqueous Flow Battery for Large-Scale Storage of Electrical Energy (Adv. Energy Mater. 8/2018). Advanced Energy Materials, 8(8), 1870034.
https://doi.org/10.1002/aenm.201870034

Yang, Z., Tong, L., Tabor, D. P., Beh, E. S., Goulet, M. A., De Porcellinis, D., Aspuru-Guzik, A., Gordon, R. G., & Aziz, M. J. (2018b). Alkaline Benzoquinone Aqueous Flow Battery for Large-Scale Storage of Electrical Energy. Advanced Energy Materials. https://doi.org/10.1002/aenm.201702056

Yu, L., Lin, F., Xiao, W., Xu, L., & Xi, J. (2019). Achieving efficient and inexpensive vanadium flow battery by combining CexZr1−xO2 electrocatalyst and hydrocarbon membrane. Chemical Engineering Journal, 356(August 2018), 622–631.
https://doi.org/10.1016/j.cej.2018.09.069

Yuan, J., Zhang, C., Qiu, Q., Pan, Z. Z., Fan, L., Zhao, Y., & Li, Y. (2022). Highly selective metal-organic framework-based (MOF-5) separator for non-aqueous redox flow battery.

Chemical Engineering Journal, 433(P2), 133564.
https://doi.org/10.1016/j.cej.2021.133564

Zai, J., Zhu, Y., He, K., Iqbal, A., Huang, S., Chen, Z., & Qian, X. (2020). Sandwiched Cu7S4@graphite felt electrode for high-performance aqueous polysulfide/iodide redox flow batteries: Enhanced cycling stability and electrocatalytic dynamics of polysulfides. Materials Chemistry and Physics, 250, 123143.
https://doi.org/10.1016/j.matchemphys.2020.123143

CHAPTER 2
LITERATURE REVIEW

Chapter 2

Literature Review

This chapter provides a brief review of the literature on electrocatalysts for redox flow batteries (RFBs), especially on Quinone-based RFBs. It starts with the RFBs as large-scale electrochemical energy storage (EES) and types of RFBs, components, working principle of Quinone-based RFB, and the role of each of the components in boosting the performance of the cell. The chapter also presents a brief review of electrocatalysts for Quinone-based RFB, gaps identified in the literature, aim and objective of the thesis.

2.1 RFBs

RFBs are of paramount importance in the context of large-scale electrochemical energy storage (EES). They offer a flexible and expandable solution for the storage of renewable energy, addressing the intermittency associated with sources such as wind and solar power. Their modular design allows for customization to fulfill the specific energy and power requirements of various applications, ranging from grid-level energy storage to remote off-grid installations. These batteries are renowned for their cost-effectiveness, utilization of non-flammable aqueous electrolytes, and extended operational lifespans, rendering them an economically viable and

eco-friendly choice. Furthermore, this battery system plays a pivotal role in enhancing grid stability, facilitating load balancing, and mitigating the necessity for costly grid infrastructure enhancements. Their sustainable characteristics align with the global shift towards cleaner energy sources, thereby reducing dependence on fossil fuels and promoting a more sustainable and robust energy landscape.

2.2 Evolution of RFBs

The RFBs have a history of more than 100 years, and the technological milestones are shown in Figure 2.1. John Doyle found the first report on Zinc-Bromine (Zn-Br) RFB in 1879 (Doyle, 1879). In the 1970s, the U.S. National Aeronautics and Space Administration (NASA) developed an Iron-Chromium RFB system (Thaller, 1976) utilizing Fe^{3+}/Fe^{2+} and Cr^{3+}/Cr^{2+} redox couples for the positive and negative sides, respectively.

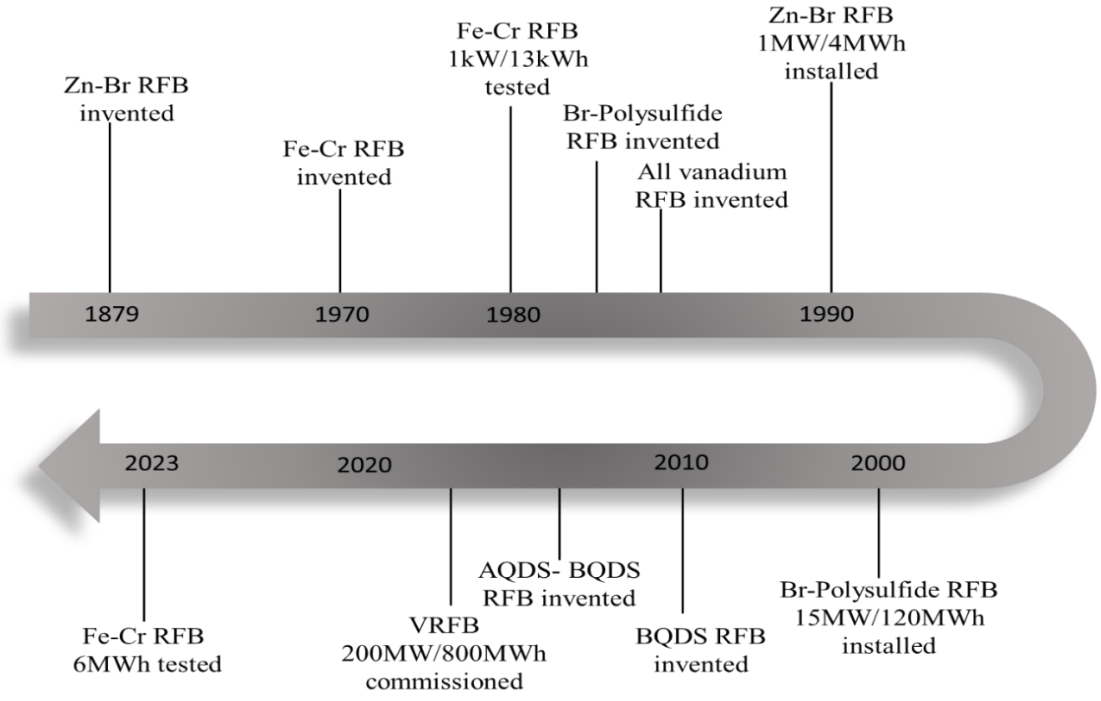

Figure 2.1 Timeline of RFB development

The prototype faced issues related to active material crossover and capacity decay, prompting the exploration of mixed electrolytes for both sides to address these challenges. The revolutionary all-vanadium RFB (VRFB) was proposed by Skyllas-Kazacos, University of New South Wales, Australia, in 1986 (Skyllas-Kazacos et al., 1986). Since then, the ongoing advancements have led to the commercialization of VRFBs. Recently, a 400 MWh capacity plant was installed and commissioned as a first phase of the bigger plant of 800MWh capacity (Tolmachev, 2022). The major classes of RFB technologies like Zn-Br, Fe-Cr, Br-polysulfide, all vanadium, and quinone redox chemistries are explained below in detail.

2.2.1 Zn-Br RFB

Zinc has emerged as a highly attractive electrolyte material and has been extensively explored in Zn-Br RFBs. Zinc is abundantly available and cost-effective. The high negative redox potential of zinc/zincate coupled with the high water solubility gives the flexibility in choosing distinct materials for positive half-cell reactions (Park et al., 2019). The Zn-Br RFB has high energy density and elevated cell voltage (P. Xu et al., 2022). The carbon electrodes and active electrolytes in Zn-Br RFB amount to an approximate cost of $8 per kWh. The electric energy cost of the battery is competitive at around $200 per kWh (Alghamdi et al., 2023). The major limitations of Zn-Br RFBs are Zn crossover and dendrite formation. Increased mass transfer of Zn ion could be a possible solution to avoid the dendrite (Xie et al., 2018). The working principle of including half-cell reactions is illustrated in Figure 2.2. Zn-Br RFB is particularly well-suited for the storage of renewable energy. Notably, Meidensha Electric Co. achieved significant success in Japan with MW-scale Zn-Br RFB as part of its Moonlight Project during the 1980s and early 1990s, completing more than 1300 cycles with an impressive 66% energy efficiency (Leung et al., 2012). Additionally, various companies such as Redflow Ltd. and Primus Power have developed and operated field installations utilizing Zn-Br RFB,

highlighting their practicality and real-world applicability in energy storage solutions (Alghamdi et al., 2023).

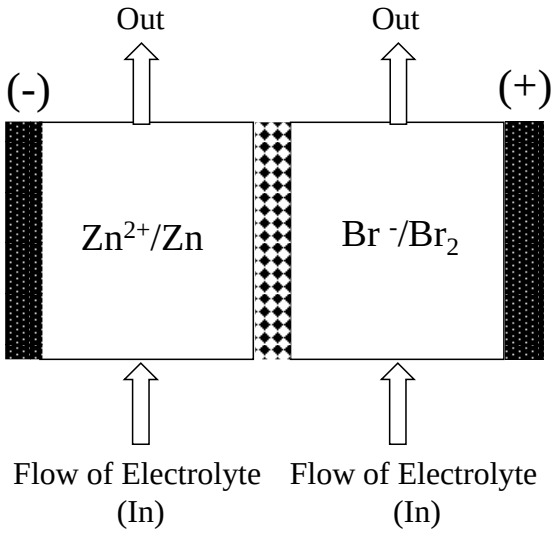

Figure 2.2 Schematic of Zn-Br RFB

$$\text{Negative Side: } Zn \underset{\text{Charge}}{\overset{\text{Discharge}}{\rightleftharpoons}} Zn^{2+} + 2e^{-} \quad \ldots\ldots (2.1) \qquad E^{0} = -0.76\ V \text{ vs SHE}$$

$$Positive\ Side: Br_2 + 2e^{-} \underset{\text{Charge}}{\overset{\text{Discharge}}{\rightleftharpoons}} 2Br^{-} \quad \ldots\ldots (2.2) \quad E^{0} = +1.087\ V \text{ vs SHE}$$

$$Overall: Br_2 + Zn \underset{\text{Charge}}{\overset{\text{Discharge}}{\rightleftharpoons}} 2Br^{-} + Zn^{2+} \quad \ldots\ldots (2.3) \quad E^{0} = +1.847\ V \text{ vs SHE}$$

2.2.2 Fe-Cr RFB

Iron and chromium are economically viable and abundant. Carbon paper, carbon cloth, and graphite felt electrodes with Bismuth catalysts on them, along with the Nafion membranes, are mostly employed in Fe-Cr RFB (Ren et al., 2023).

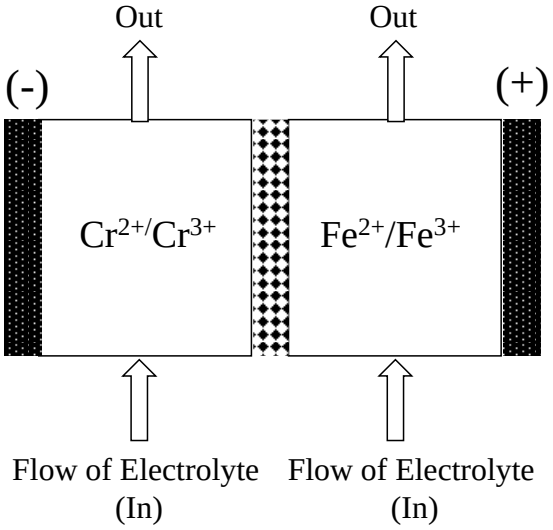

Figure 2.3 Schematic of Fe-Cr RFB

$$\text{Negative Side: } Cr^{2+} \underset{\text{Charge}}{\overset{\text{Discharge}}{\rightleftharpoons}} Cr^{3+} + e^{-} \ldots (2.4) \qquad E^0 = -0.41\,V \text{ vs SHE}$$

$$\text{Positive Side: } Fe^{3+} + e^{-} \underset{\text{Charge}}{\overset{\text{Discharge}}{\rightleftharpoons}} Fe^{2+} \ldots . (2.5) \quad E^0 = +.77\,V \text{ vs SHE}$$

$$\text{Overall: } Fe^{3+} + Cr^{2+} \underset{\text{Charge}}{\overset{\text{Discharge}}{\rightleftharpoons}} Fe^{2+} + Cr^{3+} \ldots . . (2.6) \quad E^0 = +1.18\,V \text{ vs SHE}$$

In the 1970s, during the early stages of research in Fe-Cr RFB, the crossover of active materials resulted in an irreversible loss of capacity. Scientists made a pivotal advancement by formulating a mixed iron/chromium electrolyte designed for application on both sides of the RFB (Gahn et al., 1985). However, the Fe-Cr RFB system is limited by its sluggish electrochemical kinetics associated with the Cr^{2+}/Cr^{3+} redox reaction. Additionally, on the negative side, the hydrogen evolution reaction (HER) hinders the performance. It diminishes the overall energy efficiency of the system and shows capacity degradation. In order to address the limitations, novel electrocatalysts, including Bismuth (Bi) and Gold-Thallium (Au-Tl), have been developed to enhance the electrochemical kinetics of the Cr^{2+}/Cr^{3+} redox process and

inhibit hydrogen evolution (Cheng & Hollax, 1985; Wu et al., 1986). The world's largest Fe-Cr RFB has been successfully tested in China and can store 6000 kWh of electricity for 6 hours.

2.2.3 All-Vanadium redox flow batteries (VRFB)

The VRFB is a relatively mature technology and promising among the RFB systems. It employs four oxidation states (V^{2+}, V^{3+}, V^{4+}, and V^{5+}) of vanadium dissolved in H_2SO_4 supporting electrolyte. The negolyte, V^{2+}/V^{3+} is employed, while the posolyte features VO^{2+}/VO_2^{+} shown in figure 2.4. The VRFB exhibits a cell voltage of 1.26 V (J. Kim & Park, 2022). The nominal cell voltage may vary between 1.15 and 1.55 V in acidic electrolytes, owing to the pH-dependent nature of the posolyte redox potential (Guo et al., 2023). To enhance the solubility and stability of vanadium cations, researchers have turned to mixed acid electrolytes. By combining hydrochloric acid and sulfuric acid, a stable temperature range spanning from -10 to 50 °C can be achieved, along with a high concentration of 2.5 M (resulting in an energy density of 40 Wh/L) (L. Li et al., 2011). The crossover of vanadium ions can have adverse effects on the expensive membranes. Fouling, where vanadium ions become irreversibly trapped in the membrane, can elevate cell resistance, underscoring the pressing need for cost-effective, highly selective membranes (Zhao et al., 2023). The widely used electrodes for VRFB are graphite felt, carbon felt, and carbon paper (He et al., 2022), and the membrane is Nafion (Tempelman et al., 2020). Vanadium redox flow batteries have garnered significant attention commercialized. Remarkably, a 200 MW/800 MWh VRFB—the largest of its kind in the world has been commissioned by Rongke Power in Dalian city (china) (Weaver, 2017). The current market price of vanadium electrolyte is considered relatively high at 125$/kWh (Rodby et al., 2023), and VO^{2+}/VO_2^{+} has the issue of precipitating. These remained as challenges for VRFB technology.

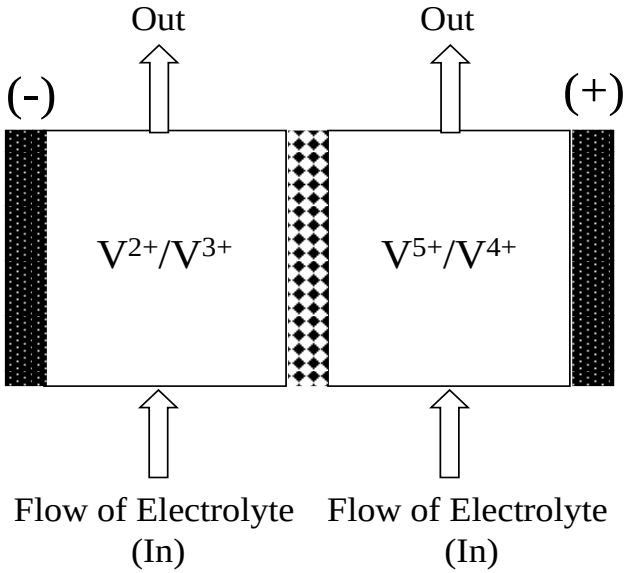

Figure 2.4 Schematic of VRFB

$$\text{Negative Side: } V^{2+} \underset{\text{Charge}}{\overset{\text{Discharge}}{\rightleftharpoons}} V^{3+} + e^{-} \ldots.(2.7) \qquad E^0 = -0.26\,V \text{ vs SHE}$$

$$\text{Positive Side: } VO_2{}^{+} + 2H^{+} + e^{-} \underset{\text{Charge}}{\overset{\text{Discharge}}{\rightleftharpoons}} VO^{2+} + H_2O \ldots.(2.8) \qquad E^0 = +1.0\,V \text{ vs SHE}$$

$$\text{Overall: } VO_2{}^{+} + V^{2+} + 2H^{+} \underset{\text{Charge}}{\overset{\text{Discharge}}{\rightleftharpoons}} VO^{2+} + V^{2+} + H_2O \ldots.(2.9) \qquad E^0 = +1.26\,V \text{ vs SHE}$$

2.2.4 Br-Polysulfide RFB

The high water solubility of alkali metal sulfide and polysulfide compounds makes them a compelling candidate for redox flow batteries. The standardized redox potential of the sulfur sulfide/polysulfide pair, which rests at approximately -0.51 V vs. SHE, is used as an anolyte (X. Wei et al., 2016). Diverse catholyte chemistries are available for this battery (i.e., ferrocyanide, iodide bromide) (Ma et al., 2019; Su et al., 2017; Wang et al., 2018). The schematic of Br-polysulfide RFB is shown in Figure 2.5. The challenges associated with the anolyte lie in its sluggish kinetics and crossover of sulfur species. The cobalt-doped carbon

electrode (X. Wei et al., 2016) and carbon-coated Nafion membrane (Su et al., 2017) were proposed to address the mentioned limitations. However, the system showed high resistance and a drop in capacity after a few cycles (Z. Li & Lu, 2021).

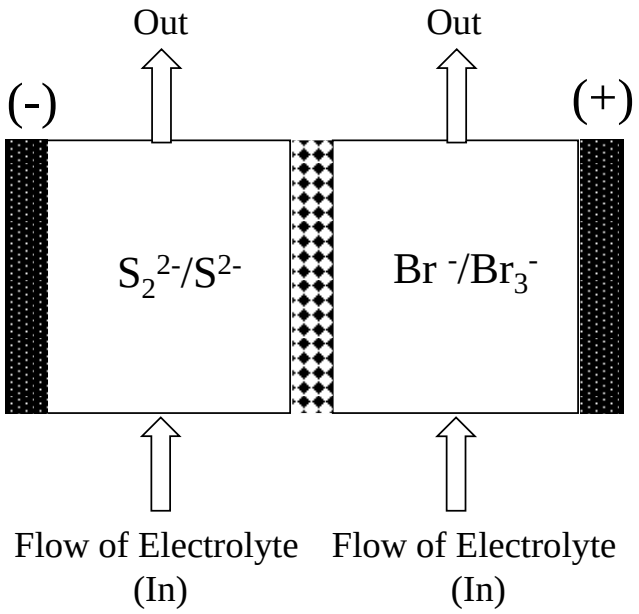

Figure 2.5 Schematic of Br-polysulfide RFB

$$\text{Negative Side: } 2S^{2-} \underset{\text{Charge}}{\overset{\text{Discharge}}{\rightleftharpoons}} S_2^{2-} + 2e^- \quad \ldots(2.10) \qquad E^0 = -0.51\,V \text{ vs SHE}$$

$$Positive\ Side: \quad Br_3^- + 2e^- \underset{\text{Charge}}{\overset{\text{Discharge}}{\rightleftharpoons}} 3Br^- \quad \ldots(2.11) \quad E^0 = +1.05\,V \text{ vs SHE}$$

$$Overall: 2S^{2-} + Br_3^- \underset{\text{Charge}}{\overset{\text{Discharge}}{\rightleftharpoons}} S_2^{2-} + 3Br^- \quad \ldots(2.12) \quad E^0 = +1.55\,V \text{ vs SHE}$$

2.3 Organic redox flow battery

Organic molecules are explored as an alternative to vanadium to reduce the cost of the stack without compromising the performance. ORFBs are efficient, scalable and environmentally friendly energy storage systems. Organic redox active molecules have the advantages of

tunability in redox potential, solubility, diffusivity, capacity, and cycling stability (Diaz-Muñoz et al., 2018; D. Xu et al., 2021). The larger size of organic active molecules reduces the unfavorable crossover through membrane. Many organic redox active molecules have fast electrochemical kinetics with multi- electron and proton transfer which improves the power density of ORFBs (X. Yang et al., 2021). Organic redox active materials such as quinone, anthraquinone, viologens, alloxazine, and 2,2,6,6-tetramethylpiperidin-1-yl)oxyl (TEMPO) are in focus (Singh et al., 2019). Each class of these materials is unique and can be operated in wide range of pH (Orita et al., 2016). The research on ORFBs is in the early stages and a summary of important studies on ORFBs are shown in Table 2.1.

2.3.1 Quinone- based redox flow batteries

Quinones-based materials are naturally present in plants, biologically active agents, and are very economical. These redox materials possess high electrochemical reversibility and rapid reaction kinetics, having a theoretical cell potential range of 0.7-1.2V (Hofmann & Schröder, 2019; Wedege et al., 2016). They create redox-active centers that facilitate the transfer of electrons, finding applications in processes like photosynthesis and aerobic respiration/ATP synthesis (Kurreck & Huber, 1995; Scott et al., 1998). The drawbacks of quinone-based redox flow batteries include their limited solubility in aqueous solutions, which can lead to low energy density, the potential for side reactions, and sluggish kinetics for bulky quinone molecules, which reduce the overall performance (Bauer et al., 2020).

Table 2.1 A review on Organic redox flow battery

S.NO.	CATHOLYTE MATERIAL	ANOLYTE MATERIAL	MEMBRANE	ELECTRODE	PERFORMANCE	REFERENCE
1	0.4M (Ferrocenylmethyl)tri-methylammonium Chloride in 2M NaCl	0.1M 3-((9,10-dioxo-9.10-dihydroanthracen-1-yl) amino)-N,N,N-trimethylpropan-1-aminium chloride (1-DPAQCl) in 2 M NaCl	AMV Selemion	Carbon Felt	Coulombic Efficiency= 95.6% Energy Efficiency = 65%	(Xia et al., 2021)
2	0.2M Dopamine hydrochloride in 3M H_2SO_4	0.2 M vanadyl sulfates in 3 M H_2SO_4	Nafion 115 Or Nafion 212	Graphite Felt	Energy Efficiency =68.3% Coulombic Efficiency=98.5%	(Q. Liu et al., 2020)
3	0.2M $[(bpy\text{-}(CH_2)_3NMe_3)]I_2$ In 1M KI	0.2M $[(bpy\text{-}(CH_2)_3NMe_3)]I_2$ In 1M KI	low-cost microporous membrane	Carbon paper	Energy Efficiency=72%	(B. Liu et al., 2020)
4	10mM 4-NH_2-TEMPO in1.4MHAc + 0.5MNaAc + 0.5MKCl	(Poly (N-anthraquinoyl pyrrole, PAQPy)/ Graphene and nafion ionomer 9:1	Nafion 212	Toray paper	Energy Efficiency=74.5% Coulombic Efficiency =92%	(Cao et al., 2019)
5	10 mM azoB/10 mM DBMMB in 1.0 M TEATFSI/solvent (MeCN or DMF	10 mM azoB/10 mM DBMMB in 1.0 M TEATFSI/solvent (MeCN or DMF	Daramic-175	Graphite felts	Energy Efficiency= 63.5%	(D. Xu et al., 2021)
7	0.1M 1,4-di-tert butyl-2-methoxy-5-(2-methoxyethoxy) benzene in 0.5 M $TEAPF_6$/MeCN	0.1 M 3-methylbenzophenone in 0.5 M $TEAPF_6$/MeCN	Daramic 250	Carbon paper	Columbic Efficiency=94% Energy Efficiency= 66%	(Xing et al., 2020)
8	0.5M 4-trimethy lammonium-TEMPO chloride (N^{Me}TEMPO) in 2M NaCl	0.5M 1,1-bis[3-(trimethylammonio) propyl]-4,4-bipyridiniumtetrachloride ((NPr)2V) in 2M NaCl	selemion AMV anion exchange membrane	Carbon paper	Coulombic Efficiency = 99%. Energy Efficiency 87%	(Hu et al., 2018)
9	0.4M ferroce-nylmethyl) trimethylammonium chloride in 1M NaCl	0.2M quaternary ammonium protected anthraquinone in 1M NaCl	Anion exchange membrane	Carbon felt	Coulombic Efficiency = 99% Energy Efficiency = 70%	(Zhu et al., 2021)
10	2M 4,5-dihydroxybenzene-1,3-disulfonic acid (BQDS) 1M H_2SO_4	1M anthraquinone-2,6-disulfonic acid (AQDS) in 1 M H_2SO_4	Nafion 212	Vulcan-xc72 Coated Toray Carbon paper	Coulombic Efficiency = 100%. Energy Efficiency= 70%	(B. Yang et al., 2016)

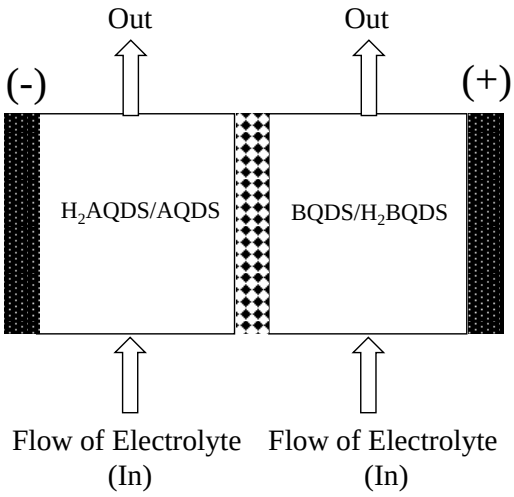

Figure 2.6 Schematic of AQDS/BQDS RFB

Negative Side Half Cell Reaction:

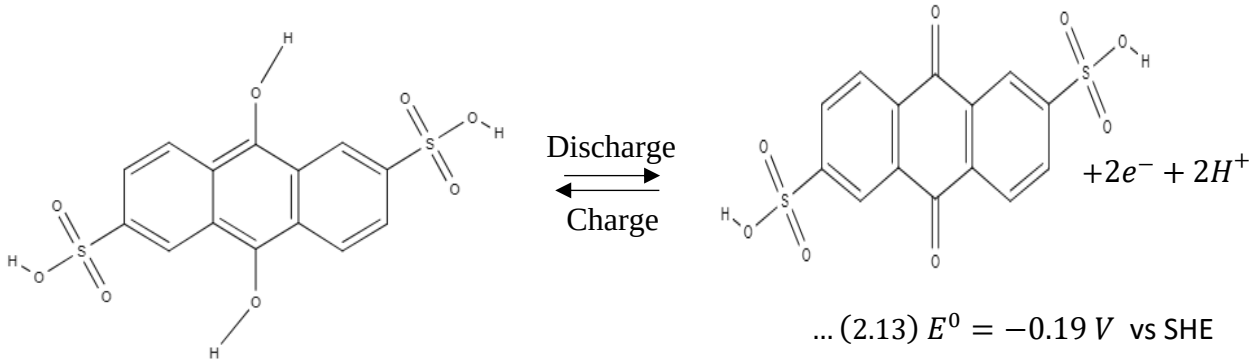

$\ldots(2.13)\ E^0 = -0.19\ V$ vs SHE

Positive Side Half Cell Reaction:

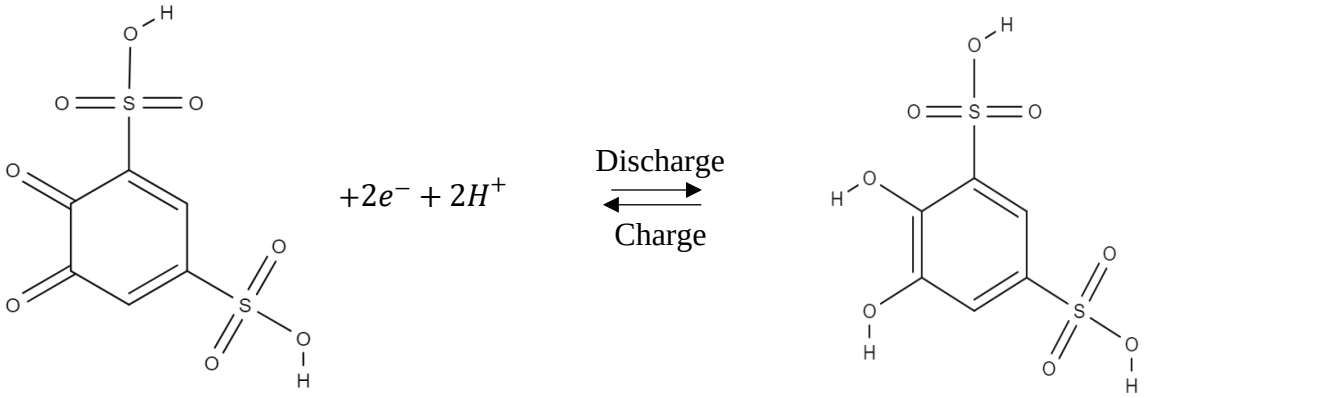

$\ldots(2.14)\ E^0 = +0.85\ V$ vs SHE

Overall Reaction:

$C_{14}H_8O_2(SO_3H)_2 + C_6H_2O_2(SO_3H)_2 \underset{\text{Charge}}{\overset{\text{Discharge}}{\rightleftharpoons}} C_{14}H_6O_2(SO_3H)_2 + C_6H_4O_2(SO_3H)_2$

(H_2AQDS) (BQDS) (AQDS) (H_2BQDS)

$\ldots(2.15)\ E^0 = +1.04V$ vs SHE

In general, carbon paper, carbon cloth, graphite felt electrodes, and membranes such as Nafion and SPEEK (Pinheiro et al., 2023) are employed in Quinone based RFBs. The 4,5-dihydroxybenzene-1,3- disulfonic acid and anthraquinone-2,6-disulfonic acid ((BQDS/AQDS) ORFB chemistry is explained in Figure 2.6.

2.4 Components of quinone-based RFB

The single cell of Quinone RFB consists of porous electrodes, membrane, bipolar plates, current collectors, and end plates, as shown in Figure 2.7. The performance of the RFB is intricately tied to the electrolytes, electrodes, and the ion-selective membrane. These components collectively underpin the overall lifespan of the RFB system. The membrane plays a crucial role in RFBs by reducing the unwanted crossover between the catholyte and anolyte while selectively facilitating the movement of charge carrier ions. The both an anion exchange membrane (AEM) and a cation exchange membrane (CEM) are used in these RFBs (J. Yuan et al., 2021).

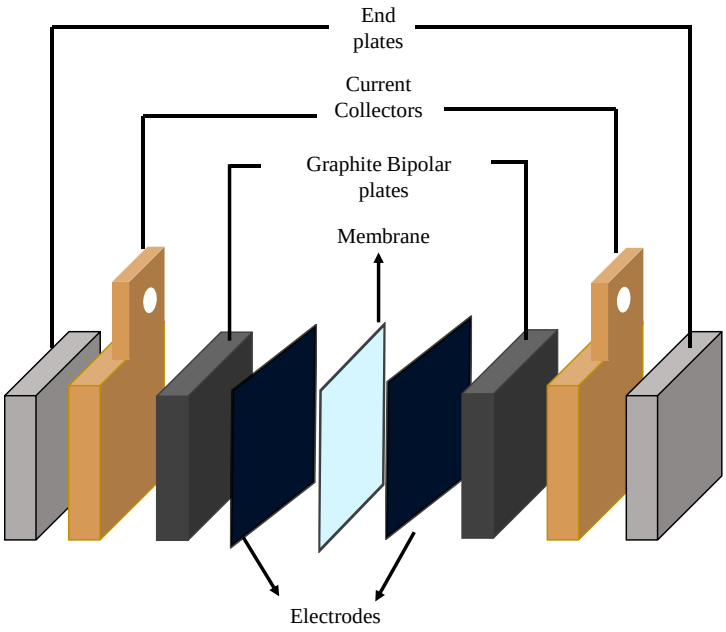

Figure 2.7 Components of a single cell of RFB

The supporting electrolyte acts as a conduit for ion movement between the positive and negative electrolyte solutions housed in separate tanks. The ideal RFB electrodes should possess optimal porosity, large surface area, favorable wetting properties for electrolytes, and minimal electronic resistance. Each of the components of the cell are explained below in detail.

2.4.1 Membrane

Within the domain of RFBs, membranes stand as indispensable components, orchestrating the intricate ballet of selective ion transport while staunchly guarding against the unwanted crossover of active materials. Given the caustic and oxidative milieu of electrolytes laden with quinone, the onus on membranes is weighty—they must exhibit not only exceptional chemical stability but also wield a prowess in ion conductivity, all while minimizing the pernicious effects of material crossover, (J. Yuan et al., 2022). Presently, the venerable Nafion membrane reigns supreme as the go-to choose for quinone-based flow batteries. However, its hegemony is not without shortcomings (Dai et al., 2021). The widespread embrace of Nafion tends to usher in elevated levels of ohmic resistance and financial costs, casting a shadow on its otherwise sterling reputation. The landscape of membrane selection in quinone RFBs is a tapestry woven with diverse alternatives, each vying to strike the delicate balance between performance and practicality. Among these contenders, sulfonated poly(ether ether ketone) (SPEEK) membranes emerge as formidable challengers, boasting a track record of enhanced efficacy (De Porcellinis et al., 2018). Additionally, the quest for affordability and functionality has spurred exploration into novel avenues, including the integration of poly(ether sulfone) (PES) porous membranes fortified with SPEEK polymer (Chen et al., 2020). Meanwhile, the emergence of alginate-based membranes presents a tantalizing prospect, offering a commendable parity in voltage efficiency (e.g., 73%) when juxtaposed with the venerable Nafion membrane (Permatasari et al., 2023). Nonetheless, this narrative is but a snapshot of an evolving saga, with the horizon of research perpetually ablaze with the fervent pursuit of the

ultimate membrane solution tailored to the exacting demands of RFB systems—a testament to the indomitable spirit of innovation and progress that animates the scientific community.

2.4.2 Electrode and electrocatalyst

In the intricate landscape of RFBs, the dynamic interplay of soluble electroactive species is paramount, undergoing chemical redox reactions at the critical junctures of membranes and electrodes (Park et al., 2016a). In the pursuit of providing active sites for these electrochemical reactions, carbonaceous electrodes, such as carbon felt and carbon papers, stand as stalwart contenders, widely employed in RFB configurations (L. Wei et al., 2023). However, the electrochemical activity of carbon electrodes, a linchpin in the efficacy of RFBs, harbors inherent limitations, often manifesting as undesirable overpotentials and the potential for water electrolysis (K. J. Kim et al., 2015). This has spurred extensive research endeavors, dedicated to surface modifications aimed at enhancing the performance of carbon electrodes within the realm of RFBs.

Commercially available carbon felt materials, sourced from diverse origins, have exhibited distinct electrochemical performances in the intricate dance of redox reactions (Banerjee et al., 2019). The challenge lies in optimizing these carbon electrodes to surmount their inherent limitations and bolster their electrochemical activity. A key avenue of exploration involves refining the wettability of carbon electrodes, a crucial factor that expedites ion transport at the electrode-electrolyte interfaces. Augmenting electrochemical activity is achieved by increasing the number of active sites, a facet critical for the overall efficiency of RFBs (Park et al., 2016b). A comprehensive overview of electrodes employed in quinone RFBs, as presented in Table 2.2, illuminates the prevalent reliance on carbon-based materials. These materials, owing to their intrinsic qualities of strong acid resistance, high conductivity, and cost-effectiveness, emerge as preferred choices in RFB applications (Yue et al., 2010). However, their hydrophilic nature and relatively low electrochemical activity impose limitations, necessitating careful

consideration and modification before their seamless integration into battery systems (Xian et al., 2021).

The environmental conditions within RFBs present a formidable challenge to electrode materials. Operating in a highly acidic environment and contending with strong oxidizing conditions, the selected electrode material must not only exhibit robust acid resistance but also withstand the corrosive forces at play (Yue et al., 2010). Carbon-based materials, in meeting these stringent criteria, become natural contenders due to their durability and cost-effectiveness. Yet, their hydrophilic tendencies and modest electrochemical activity necessitate judicious intervention.

The modification of carbon-based electrodes before their deployment in battery applications is a critical step in unleashing their full potential. Various techniques, encompassing both physical and chemical treatments, are employed to refine the inherent properties of carbon-based materials. These modifications are geared towards overcoming the challenges posed by their hydrophilic nature and enhancing their electrochemical activity. Physical treatments may include processes such as heat treatment or the introduction of conductive additives to enhance the electrical conductivity of the carbon matrix. These physical interventions serve to optimize the electron transport pathways within the electrode structure, contributing to improved electrochemical performance (Xian et al., 2021). Chemical treatments, on the other hand, encompass a spectrum of methodologies, including surface functionalization and the incorporation of heteroatoms into the carbon matrix. The objective is to tailor the surface properties of carbon electrodes, transforming their hydrophilic nature into a more hydrophobic state. This alteration not only mitigates issues related to water electrolysis but also enhances the overall electrochemical activity, fostering a conducive environment for redox reactions.

In essence, the quest for optimizing carbon-based electrodes for RFB applications necessitates a holistic approach, encompassing physical and chemical modifications. The intricacies of

electrode performance are intertwined with the subtleties of their surface characteristics, and fine-tuning these properties is instrumental in overcoming the challenges posed by their hydrophilic nature. This multidimensional strategy holds the promise of unlocking the full potential of carbon-based electrodes in the domain of RFBs, paving the way for enhanced efficiency and prolonged operational lifespans in the realm of energy storage technologies. In recent years, the integration of catalysts has become a key focal point, particularly in the exploration of both metals and metal oxides. Among these, titanium dioxide (TiO_2) and tungsten trioxide (WO_3) have emerged as captivating inorganic metal oxides, drawing significant attention for their remarkable electrochemical and catalytic abilities (Hua et al., 2019; L. Wei et al., 2023; W. Zhang et al., 2021). What sets these materials apart is not only their electrochemical prowess but also their notable attributes of chemical stability, non-toxicity, and cost-effectiveness, distinguishing them from other metal oxides. (Calvo et al., 2001; Sadeghzadeh Attar et al., 2008). The appeal of TiO_2 and WO_3 lies not only in their inherent characteristics but also in their potential to address challenges faced by other metal oxides commonly used in electrocatalysis. IrO_2 and RuO_2, while effective, often come with a higher cost and potential toxicity concerns. The utilization of TiO_2 and WO_3, with their favorable attributes, presents a promising avenue for overcoming these limitations, making them a subject of substantial interest in the field. One of the pivotal requirements for effective electrocatalysis is the attainment of a high surface area. Both TiO_2 and WO_3 excel in this aspect, providing ample sites for electrochemical reactions to take place. This high surface area facilitates swift electrochemical reactions and ensures superior mass transport of active species, contributing to excellent rate capability and enhanced battery efficiency (Zhou et al., 2017). The ability of these metal oxides to actively participate in the redox processes highlights their potential to be game-changers in the realm of electrocatalysis, specifically within the context of redox flow chemistry.

Metal oxide-based catalysts, particularly those centered around TiO_2 and WO_3, present themselves as active and economical solutions. Their exploration as potential remedies to the sluggish kinetics inherent in redox flow chemistry is particularly promising. Despite the immense promise, it's essential to acknowledge the need for comprehensive exploration and understanding of these catalysts' behavior in the specific context of redox flow chemistry. Factors such as their long-term stability, compatibility with different electrolyte systems, and scalability must be thoroughly investigated to unlock their full potential.

Table 2.2 Summary of membrane, electrode materials used and their influence on performance of Quinone-based RFBs

S.No.	Battery system	Membrane	Electrodes	Performance	Ref
1.	Alizarin red (ARS)/ferro-ferricyanide	Nafion 212	Carbon Felt	CE=99 %, EE=84 %	(Chen et al., 2020)
2.	Alizarin red (ARS)/ferro-ferricyanide	PES with SPEEK	Carbon Felt	CE=98 %, EE=85 %	(Chen et al., 2020)
3.	Dihydroxyanthraquinone/ferro-ferricyanide	SPEEK	Carbon Paper	EE=66%	(De Porcellinis et al., 2018)
4.	Dihydroxyanthraquinone/ferro-ferricyanide	Nafion	Carbon Paper	EE=59%	(De Porcellinis et al., 2018)
5.	TironA/2,7-anthraquinone disulfonic acid	Alginate based	Carbon Felt	VE=74.3%	(Permatasari et al., 2023)
6.	TironA/2,7-anthraquinone disulfonic acid	Nafion	Carbon Felt	VE=73%	(Permatasari et al., 2023)
7.	ARS/ BQDS	Nafion	Carbon Felt	EE=45%	(Pinheiro et al., 2023)
8.	ARS / BQDS	SPEEK	Carbon Felt	EE=51%	(Pinheiro et al., 2023)
9	AQDS/BQDS	Nafion 212	Vulcan-xc72 Coated Toray Carbon paper	CE = 100%. EE= 70%	(B. Yang et al., 2016)

2.5 Gaps identified in the literature

After carefully going through the literature, some of the major limitations in the present literature on ORFBs are reported below:

1. High cost of Vanadium electrolyte opened the venues to explore alternative active materials.
2. The few works only reported on quinone based redox flow battery.
3. No work has been reported on electrocatalyst materials for quinone based redox flow battery.
4. Non-Precious electrocatalysts have not explored till date.

2.6 Aim and objectives

Aim: To develop non-noble electrocatalysts for quinone based redox flow battery.

The following are the detailed objectives.

1. Selection of quinone redox couple for redox flow battery system.
2. Evaluation of non-noble electrocatalysts.
3. Development of TiO_2@CNP electrocatalyst for positive half-cell of H_2-BQ redox flow battery. (P1)
4. Development of WO_3/C electrocatalyst for HQ-BQ RFB redox flow batteries.
5. Testing and comparative performance evaluation of TiO_2@CNP and WO_3/C in H_2-BQ and HQ-BQ redox flow batteries.

References

Alghamdi, N. S., Rana, M., Peng, X., Huang, Y., Lee, J., Hou, J., Gentle, I. R., Wang, L., & Luo, B. (2023). Zinc–Bromine Rechargeable Batteries: From Device Configuration, Electrochemistry, Material to Performance Evaluation. In *Nano-Micro Letters* (Vol. 15, Issue 1). Springer Nature Singapore.
https://doi.org/10.1007/s40820-023-01174-7

Banerjee, R., Bevilacqua, N., Mohseninia, A., Wiedemann, B., Wilhelm, F., Scholta, J., & Zeis, R. (2019). Carbon felt electrodes for redox flow battery: Impact of compression on transport properties. *Journal of Energy Storage*, *26*, 100997. https://doi.org/10.1016/j.est.2019.100997

Bauer, S., Namyslo, J. C., Kaufmann, D. E., & Turek, T. (2020). Evaluation of Options and Limits of Aqueous All-Quinone-Based Organic Redox Flow Batteries. *Journal of The Electrochemical Society*, *167*(11), 110522.
https://doi.org/10.1149/1945-7111/aba338

Calvo, M. E., Candal, R. J., & Bilmes, S. A. (2001). Photooxidation of Organic Mixtures on Biased TiO2 Films. *Environmental Science & Technology*, *35*(20), 4132–4138. https://doi.org/10.1021/es010613r

Cao, J., Ding, F., Chen, H., Wang, H., Wang, W., Chen, Z., & Xu, J. (2019). A new redox-active conjugated polymer containing anthraquinone pendants as anode material for aqueous all-organic hybrid-flow battery. *Journal of Power Sources*. https://doi.org/10.1016/j.jpowsour.2019.03.098

Chen, D., Duan, W., He, Y., Li, T., Kang, C., Dai, Q., Yuan, Z., & Li, X. (2020). Porous Membrane with High Selectivity for Alkaline Quinone-Based Flow Batteries. *ACS Applied Materials & Interfaces*, *12*(43), 48533–48541.
https://doi.org/10.1021/acsami.0c13172

Cheng, D. S., & Hollax, E. (1985). The Influence of Thallium on the Redox Reaction Cr3+/Cr2+. *Journal of The Electrochemical Society*, *132*(2), 269–273. https://doi.org/10.1149/1.2113807

Dai, Q., Zhao, Z., Shi, M., Deng, C., Zhang, H., & Li, X. (2021). Ion conductive membranes for flow batteries: Design and ions transport mechanism. *Journal of Membrane Science*, *632*(April), 119355.
https://doi.org/10.1016/j.memsci.2021.119355

De Porcellinis, D., Mecheri, B., D'Epifanio, A., Licoccia, S., Granados-Focil, S., & Aziz, M. J. (2018). Communication—Sulfonated Poly (ether ether ketone) as Cation Exchange Membrane for Alkaline Redox Flow Batteries. *Journal of The Electrochemical Society*, *165*(5), A1137.
https://doi.org/10.1149/2.1291805jes

Diaz-Muñoz, G., Miranda, I. L., Sartori, S. K., de Rezende, D. C., & Diaz, M. A. N. (2018). *Chapter 11 - Anthraquinones: An Overview* (B. T.-S. in N. P. C. Atta-ur-Rahman (ed.); Vol. 58, pp. 313–338). Elsevier.
https://doi.org/10.1016/B978-0-444-64056-7.00011-8

Doyle. (1879). Galvanic Batteries. *Scientific American*, *7*(159supp), 2525–2528. https://doi.org/10.1038/scientificamerican01181879-2525csupp

Gahn, R. F., Hagedorn, N. H., & Johnson, J. A. (1985). *Cycling performance of the iron-chromium redox energy storage system*.
https://www.osti.gov/biblio/5325610

González, Z., Botas, C., Álvarez, P., Roldán, S., Blanco, C., Santamaría, R., Granda, M., & Menéndez, R. (2012). Thermally reduced graphite oxide as positive electrode in Vanadium Redox Flow Batteries. *Carbon*, *50*(3), 828–834. https://doi.org/10.1016/j.carbon.2011.09.041

Guo, Y., Huang, J., & Feng, J.-K. (2023). Research progress in preparation of electrolyte for all-vanadium redox flow battery. *Journal of Industrial and Engineering Chemistry*, *118*, 33–43.
https://doi.org/10.1016/j.jiec.2022.11.037

He, Z., Lv, Y., Zhang, T., Zhu, Y., Dai, L., Yao, S., Zhu, W., & Wang, L. (2022). Electrode materials for vanadium redox flow batteries: Intrinsic treatment and introducing catalyst. *Chemical Engineering Journal*, *427*, 131680.
https://doi.org/10.1016/j.cej.2021.131680

Hofmann, J. D., & Schröder, D. (2019). Which Parameter is Governing for Aqueous Redox Flow Batteries with Organic Active Material? *Chemie-Ingenieur-Technik*, *91*(6), 786–794. https://doi.org/10.1002/cite.201800162

Hu, B., Tang, Y., Luo, J., Grove, G., Guo, Y., & Liu, T. L. (2018). Improved radical stability of viologen anolytes in aqueous organic redox flow batteries. *Chemical Communications*. https://doi.org/10.1039/c8cc02336k

Hua, C., Yuan, G., Cheng, Z., Jiang, H., Xu, G., Liu, Y., & Han, G. (2019). Building architecture of TiO2 nanocrystals embedded in amorphous WO3 films with improved electrochromic properties. *Electrochimica Acta*, *309*, 354–361. https://doi.org/10.1016/j.electacta.2019.04.063

Jiang, Y., Cheng, G., He, Z., Chen, J., Li, Y., Zhu, J., Meng, W., Zhou, H., Dai, L., & Wang, L. (2019). Biomass-Derived Porous Graphitic Carbon with Excellent Electrocatalytic Performances for Vanadium Redox Reactions. *Journal of The Electrochemical Society*, *166*(16), A3918–A3926.
https://doi.org/10.1149/2.0941915jes

Kim, J., & Park, H. (2022). Recent advances in porous electrodes for vanadium redox flow batteries in grid-scale energy storage systems : A mass transfer perspective. *Journal of Power Sources*, *545*(July), 231904.
https://doi.org/10.1016/j.jpowsour.2022.231904

Kim, K. J., Park, M.-S., Kim, Y.-J., Kim, J. H., Dou, S. X., & Skyllas-Kazacos, M. (2015). A technology review of electrodes and reaction mechanisms in vanadium redox flow batteries. *Journal of Materials Chemistry A*, *3*(33), 16913–16933.
https://doi.org/10.1039/C5TA02613J

Kurreck, H., & Huber, M. (1995). Model Reactions for Photosynthesis—Photoinduced Charge and Energy Transfer between Covalently Linked Porphyrin and Quinone Units. In *Angewandte Chemie International Edition in English*.
https://doi.org/10.1002/anie.199508491

Leung, P., Li, X., Ponce de Leon, C., Berlouis, L., Low, C. T. J., & Walsh, F. C. (2012). Progress in redox flow batteries, remaining challenges and their applications in energy storage. *RSC Adv.*, *2*, 10125.
https://doi.org/10.1039/C2RA21342G

Li, L., Kim, S., Wang, W., Vijayakumar, M., Nie, Z., Chen, B., Zhang, J., Xia, G., Hu, J., Graff, G., Liu, J., & Yang, Z. (2011). A stable vanadium redox-flow battery with high energy density for large-scale energy storage. *Advanced Energy Materials*. https://doi.org/10.1002/aenm.201100008

Li, Z., & Lu, Y.-C. (2020). Material Design of Aqueous Redox Flow Batteries: Fundamental Challenges and Mitigation Strategies. *Advanced Materials*, *32*(47), 2002132. https://doi.org/10.1002/adma.202002132

Li, Z., & Lu, Y.-C. (2021). Polysulfide-based redox flow batteries with long life and low levelized cost enabled by charge-reinforced ion-selective membranes. *Nature Energy*, *6*(5), 517–528.
https://doi.org/10.1038/s41560-021-00804-x

Liu, B., Tang, C. W., Jiang, H., Jia, G., & Zhao, T. (2020). An aqueous organic redox flow battery employing a trifunctional electroactive compound as anolyte, catholyte and supporting electrolyte. *Journal of Power Sources*.
https://doi.org/10.1016/j.jpowsour.2020.228985

Ma, D., Hu, B., Wu, W., Liu, X., Zai, J., Shu, C., Tadesse Tsega, T., Chen, L., Qian, X., & Liu, T. L. (2019). Highly active nanostructured CoS2/CoS heterojunction electrocatalysts for aqueous polysulfide/iodide redox flow batteries. *Nature Communications*, *10*(1), 3367. https://doi.org/10.1038/s41467-019-11176-y

Orita, A., Verde, M. G., Sakai, M., & Meng, Y. S. (2016). The impact of pH on side reactions for aqueous redox flow batteries based on nitroxyl radical compounds. *Journal of Power Sources*, *321*, 126–134.
https://doi.org/https://doi.org/10.1016/j.jpowsour.2016.04.136

Park, M., Beh, E. S., Fell, E. M., Jing, Y., Kerr, E. F., De Porcellinis, D., Goulet, M. A., Ryu, J., Wong, A. A., Gordon, R. G., Cho, J., & Aziz, M. J. (2019). A High Voltage Aqueous Zinc–Organic Hybrid Flow Battery. *Adv. Energy Mater.*, *9*, 1900694.
https://doi.org/10.1002/aenm.201900694

Park, M., Ryu, J., Wang, W., & Cho, J. (2016a). Material design and engineering of next-generation flow-battery technologies. In *Nature Reviews Materials*. https://doi.org/10.1038/natrevmats.2016.80

Park, M., Ryu, J., Wang, W., & Cho, J. (2016b). Material design and engineering of next-generation flow-battery technologies. *Nat. Rev. Mater.*, *2*(1), 16080.
https://doi.org/10.1038/natrevmats.2016.80

Permatasari, A., Mara Ikhsan, M., Henkensmeier, D., & Kwon, Y. (2023). Utilization of novel alginate membranes developed for quinone based aqueous redox flow batteries. *Journal of Industrial and Engineering Chemistry*, *122*, 264–273. https://doi.org/https://doi.org/10.1016/j.jiec.2023.02.027

Pinheiro, D., Sousa, J. F. M., Pineiro, M., Valente, A. J. M., & Seixas de Melo, J. S. (2023). Non-pre-treated sulfonated poly(ether ether ketone) membrane as an efficient alternative for Nafion in acidic aqueous organic redox flow batteries. *Journal of Energy Storage*, *57*, 106201. https://doi.org/https://doi.org/10.1016/j.est.2022.106201

Ren, H., Su, Y., Zhao, S., Li, C., Wang, X., Li, B., & Li, Z. (2023). Research on the Performance of Cobalt Oxide Decorated Graphite Felt as Electrode of Iron-Chromium Flow Battery. *ChemElectroChem*, *10*(5), e202201146. https://doi.org/10.1002/celc.202201146

Rodby, K. E., Jaffe, R. L., Olivetti, E. A., & Brushett, F. R. (2023). Materials availability and supply chain considerations for vanadium in grid-scale redox flow batteries. *Journal of Power Sources*, *560*, 232605. https://doi.org/10.1016/j.jpowsour.2022.232605

Sadeghzadeh Attar, A., Sasani Ghamsari, M., Hajiesmaeilbaigi, F., Mirdamadi, S., Katagiri, K., & Koumoto, K. (2008). Synthesis and characterization of anatase and rutile TiO2 nanorods by template-assisted method. *Journal of Materials Science*, *43*(17), 5924–5929. https://doi.org/10.1007/s10853-008-2872-y

Scott, D. T., Mcknight, D. M., Blunt-Harris, E. L., Kolesar, S. E., & Lovley, D. R. (1998). Quinone moieties act as electron acceptors in the reduction of humic substances by humics-reducing microorganisms. *Environmental Science and Technology*. https://doi.org/10.1021/es980272q

Singh, V., Kim, S., Kang, J., & Byon, H. R. (2019). Aqueous organic redox flow batteries. *Nano Research*, *12*(9), 1988–2001. https://doi.org/10.1007/s12274-019-2355-2

Skyllas-Kazacos, M., Rychcik, M., Robins, R. G., Fane, A. G., & Green, M. A. (1986). New All-Vanadium Redox Flow Cell. *Journal of The Electrochemical Society*. https://doi.org/10.1149/1.2108706

Su, L., Badel, A. F., Cao, C., Hinricher, J. J., & Brushett, F. R. (2017). Toward an Inexpensive Aqueous Polysulfide–Polyiodide Redox Flow Battery. *Industrial & Engineering Chemistry Research*, *56*(35), 9783–9792. https://doi.org/10.1021/acs.iecr.7b01476

Tempelman, C. H. L., Jacobs, J. F., Balzer, R. M., & Degirmenci, V. (2020). Membranes for all vanadium redox flow batteries. *Journal of Energy Storage*, *32*, 101754. https://doi.org/10.1016/j.est.2020.101754

Thaller, L. H. (1976). *ELECTRICALLY RECHARGEABLE REDOX FLOW CELLS.*

Tolmachev, Y. V. (2022). *Flow Batteries From 1879 To 2022 And Beyond. Yuriy V. Tolmachev 1*. 1–79. https://doi.org/10.32388/G6G4EA

Wang, L., Wang, X., Liu, J., Yang, H., Fu, C., Xia, Y., & Liu, T. (2018). A rechargeable metal-free full-liquid sulfur–bromine battery for sustainable energy storage. *Journal of Materials Chemistry A*, *6*(42), 20737–20745. https://doi.org/10.1039/C8TA07951J

Wedege, K., Dražević, E., Konya, D., & Bentien, A. (2016). Organic Redox Species in Aqueous Flow Batteries: Redox Potentials, Chemical Stability and Solubility. *Scientific Reports*, *6*(1), 39101.
https://doi.org/10.1038/srep39101

Wei, L., Zeng, L., Han, M. S., Li, W. J., Chen, L. P., Xu, J. H., & Zhao, T. S. (2023). Nano TiC electrocatalysts embedded graphite felt for high rate and stable vanadium redox flow batteries. *Journal of Power Sources*, *576*, 233180. https://doi.org/10.1016/j.jpowsour.2023.233180

Wei, X., Xia, G., Kirby, B., Thomsen, E., Li, B., Nie, Z., Graff, G. G., Liu, J., Sprenkle, V., & Wang, W. (2016). An Aqueous Redox Flow Battery Based on Neutral Alkali Metal Ferri/ferrocyanide and Polysulfide Electrolytes. *J. Electrochem. Soc.*, *163*(1), A5150.
DOI 10.1149/2.0221601jes

Wu, C. D., Scherson, D. A., Calvo, E. J., Yeager, E. B., & Reid, M. A. (1986). A Bismuth-Based Electrocatalyst for the Chromous-Chromic Couple in Acid Electrolytes. *Journal of The Electrochemical Society*.
https://doi.org/10.1149/1.2108351

Xia, L., Huo, W., Gao, H., Zhang, H., Chu, F., Liu, H., & Tan, Z. (2021). Intramolecular hydrogen bonds induced high solubility for efficient and stable anthraquinone based neutral aqueous organic redox flow batteries. *Journal of Power Sources*. https://doi.org/10.1016/j.jpowsour.2021.229896

Xian, J., Ma, H., Li, Z., Ding, C., Liu, Y., Yang, J., & Cui, F. (2021). α-FeOOH nanowires loaded on carbon paper anodes improve the performance of microbial fuel cells. *Chemosphere*, *273*, 129669.
https://doi.org/10.1016/j.chemosphere.2021.129669

Xie, C., Zhang, H., Xu, W., Wang, W., & Li, X. (2018). A Long Cycle Life, Self-Healing Zinc–Iodine Flow Battery with High Power Density. *Angewandte Chemie International Edition*, *57*(35), 11171–11176.
https://doi.org/10.1002/anie.201803122

Xing, X., Liu, Q., Wang, B., Lemmon, J. P., & Xu, W. Q. (2020). A low potential solvent-miscible 3-methylbenzophenone anolyte material for high voltage and energy density all-organic flow battery. *Journal of Power Sources*. https://doi.org/10.1016/j.jpowsour.2019.227330

Xu, D., Zhang, C., Zhen, Y., Zhao, Y., & Li, Y. (2021). A high-rate nonaqueous organic redox flow battery. *Journal of Power Sources*. https://doi.org/10.1016/j.jpowsour.2021.229819

Xu, P., Li, T., Zheng, Q., Zhang, H., Yin, Y., & Li, X. (2022). A low-cost bromine-fixed additive enables a high capacity retention zinc-bromine batteries. *Journal of Energy Chemistry*, *65*, 89–93.
https://doi.org/10.1016/j.jechem.2021.05.036

Yang, B., Hoober-Burkhardt, L., Krishnamoorthy, S., Murali, A., Prakash, G. K. S., & Narayanan, S. R. (2016). High-Performance Aqueous Organic Flow Battery with Quinone-Based Redox Couples at Both Electrodes. *Journal of The Electrochemical Society*. https://doi.org/10.1149/2.1371607jes

Yang, X., Garcia, S. N., Janoschka, T., Kónya, D., Hager, M. D., & Schubert, U. S. (2021). Novel, stable catholyte for aqueous organic redox flow batteries: Symmetric cell study of

hydroquinones with high accessible capacity. *Molecules*, *26*(13). https://doi.org/10.3390/molecules26133823

Yuan, J., Pan, Z. Z., Jin, Y., Qiu, Q., Zhang, C., Zhao, Y., & Li, Y. (2021). Membranes in non-aqueous redox flow battery: A review. *Journal of Power Sources*, *500*(May), 229983. https://doi.org/10.1016/j.jpowsour.2021.229983

Yuan, J., Zhang, C., Qiu, Q., Pan, Z. Z., Fan, L., Zhao, Y., & Li, Y. (2022). Highly selective metal-organic framework-based (MOF-5) separator for non-aqueous redox flow battery. *Chemical Engineering Journal*, *433*(P2), 133564. https://doi.org/10.1016/j.cej.2021.133564

Yue, L., Li, W., Sun, F., Zhao, L., & Xing, L. (2010). Highly hydroxylated carbon fibres as electrode materials of all-vanadium redox flow battery. *Carbon*, *48*(11), 3079–3090. https://doi.org/10.1016/j.carbon.2010.04.044

Zhang, W., Zhong, Y., Wang, Q., Shen, D., & Liu, G. (2021). Comparison Study of the SCR Performance over Mn–TiO2 and Ce–TiO2 Catalysts: An Experimental and DFT Study. *Energy & Fuels*, *35*(18), 14681–14691. https://doi.org/10.1021/acs.energyfuels.1c02170

Zhao, N., Platt, A., Riley, H., Qiao, R., Neagu, R., & Shi, Z. (2023). Strategy towards high ion selectivity membranes for all-vanadium redox flow batteries. *Journal of Energy Storage*, *72*, 108321. https://doi.org/10.1016/j.est.2023.108321

Zhou, X. L., Zhao, T. S., An, L., Zeng, Y. K., & Wei, L. (2017). Critical transport issues for improving the performance of aqueous redox flow batteries. *Journal of Power Sources*, *339*, 1–12. https://doi.org/10.1016/j.jpowsour.2016.11.040

Zhu, Y., Li, Y., Qian, Y., Zhang, L., Ye, J., Zhang, X., & Zhao, Y. (2021). Anthraquinone-based anode material for aqueous redox flow batteries operating in nondemanding atmosphere. *Journal of Power Sources*. https://doi.org/10.1016/j.jpowsour.2021.229984

CHAPTER 3

EXPERIMENTAL

CHAPTER 3

EXPERIMENTAL

This chapter shows the detailed synthesis and characterization processes employed for the TiO_2@CNP and WO_3/C electrocatalysts, integral components utilized in H_2-BQ and HQ-BQ Redox Flow Batteries (RFBs). The investigation encompasses a thorough examination of various analytical techniques, including Field Emission Scanning Electron Microscope (FESEM), Fourier transform infrared spectroscopy (FTIR), X-ray diffraction (XRD), and cyclic voltammetry (CV), to elucidate the structural and chemical properties of the synthesized electrocatalysts. Furthermore, the performance evaluation of these RFBs is conducted through galvanostatic charge-discharge tests (GCD), offering insights into their electrochemical behavior and operational efficacy.

The synthesis process of TiO_2@CNP and WO_3/C electrocatalysts involves a series of precisely controlled steps aimed at achieving the desired morphological and compositional attributes conducive to enhanced electrochemical performance. These protocols entail the judicious

selection of precursor materials, optimization of reaction conditions, and careful post-treatment procedures to tailor the properties of the electrocatalysts according to the specific requirements of H_2-BQ and HQ-BQ RFB systems. Following synthesis, the electrocatalysts undergo a rigorous characterization regime to unravel their structural, morphological, and chemical characteristics. Field Emission Scanning Electron Microscope (FESEM) imaging provides invaluable insights into the surface morphology and nano-structural features of the electrocatalysts, elucidating their particle size distribution and surface topography. Fourier transform infrared spectroscopy (FTIR) offers a comprehensive analysis of the functional groups present within the electrocatalyst materials, shedding light on their chemical composition and surface chemistry. Moreover, X-ray diffraction (XRD) analysis serves as a powerful tool for elucidating the crystalline structure and phase purity of the synthesized electrocatalysts. By identifying the crystallographic phases present and quantifying their relative abundance, XRD facilitates a detailed understanding of the structural evolution and phase transitions occurring during the synthesis process. Additionally, cyclic voltammetry (CV) studies provide crucial insights into the electrochemical behavior and redox properties of the electrocatalysts, offering valuable information on their catalytic activity, stability, and kinetics. Following comprehensive characterization, the synthesized TiO_2@CNP and WO_3/C electrocatalysts are integrated into H_2-BQ and HQ-BQ RFB configurations, and their performance is evaluated through galvanostatic charge-discharge tests (GCD). These tests serve as a robust means of assessing the electrochemical performance and operational efficiency of the RFB systems, providing valuable data on parameters such as coulombic efficiency, voltage efficiency, and energy efficiency.

3.1 Materials

Benzoquinone (Sigma Aldrich), Hydroquinone, H_2SO_4 (98 wt%), sodium lauryl sulfate (SLS), sodium tungstate hydrate, activated charcoal powder, and Isopropanol (IPA) were supplied by

FINAR, India. Titanium Dioxide (Loba Chemie Pvt Ltd., India), Nafion (Sainergy fuel cell India Pvt Ltd), Toray carbon paper (Nickunj Eximp Entp Pvt Ltd, India).

3.2 Development of TiO_2@CNP and WO_3/C electrocatalyst

Electrocatalysts play a pivotal role in enhancing the electrochemical activity at the surface of the electrode, thereby significantly impacting the performance and efficiency of redox flow battery (RFB) systems. Among the plethora of materials explored for this purpose, metal oxides stand out as particularly promising candidates owing to their low cost, tunability, and high activity (Miu et al., 2022). In this context, the non-precious electrocatalysts TiO_2@CNP and WO_3/C have emerged as focal points of research, tailored specifically for application in H_2-BQ and HQ-BQ RFBs.

The synthesis of TiO_2@CNP involves a controlled process aimed at achieving the desired composition and structure conducive to enhanced electrochemical performance. Initially, a mixture of isopropyl alcohol (IPA) and water in a 1:1 ratio is prepared, serving as the solvent medium. This solvent mixture is then subjected to agitation using a stirrer for a duration of 10 minutes to ensure homogeneity and uniform dispersion of the components. Subsequently, a carefully calibrated combination of carbon nanoparticles (CNP), titanium dioxide (TiO_2), and a Nafion solution is introduced into the solvent mixture in predetermined proportions. The inclusion of CNP serves to provide a robust support matrix for anchoring the TiO_2 nanoparticles, thereby enhancing their stability and electrochemical activity. The precise ratios and concentrations of these components are optimized through iterative experimentation to achieve the desired electrochemical performance characteristics. Following the addition of the constituent materials, the resulting suspension undergoes ultrasonication for a duration of 30 minutes. This ultrasonic treatment serves to promote intimate mixing and dispersion of the components, facilitating the formation of a homogeneous TiO_2@CNP composite material. The

ultrasonication process imparts mechanical energy to the system, breaking down agglomerates and promoting the uniform distribution of TiO_2 nanoparticles on the surface of the carbon nanoparticles. The detailed synthesis procedure for TiO_2 @CNP is visually depicted in Figure 3.1, providing a comprehensive overview of the sequential steps involved in the fabrication process. This schematic representation serves as a valuable reference guide, elucidating the key stages of synthesis and highlighting the critical parameters that govern the composition and structure of the resulting electrocatalyst material. WO_3/C electrocatalyst also synthesized using a tailored approach optimized for compatibility with H_2-BQ and HQ-BQ RFB systems. The synthesis methodology for WO_3/C follows a similar framework, incorporating carbonaceous support materials and tungsten trioxide (WO_3) nanoparticles to achieve synergistic electrochemical performance. Tungsten trioxide (WO_3) nanoparticles were synthesized using the method reported in the literature (Patel et al., 2015). 1 g of Sodium tungstate dihydrate ($Na_2WO_4.2H_2O$) was dissolved in a 40 ml solution of DI water and HCl (pH = 0.5), and a small amount of sodium lauryl sulfate was added to avoid the agglomeration. This solution mixture was stirred for one hour at 65°C to complete the reactions below (1) and (2). The H_2WO_4 cake, underwent a meticulous drying process at a controlled temperature of 80°C for a duration of 6 hours, resulting in the formation of finely powdered H_2WO_4 particles. These particles were subsequently subjected to a carefully controlled environment within a tubular furnace, where they were exposed to a nitrogen atmosphere at an elevated temperature of 350°C for a duration of 2 hours. This step aimed to effectively eliminate any structurally bound moisture, thereby facilitating the transformation of the precursor particles into structurally stable WO_3 nanoparticles. Following this thermal treatment, the particle size of the synthesized WO_3 nanoparticles was meticulously characterized at ambient room temperature using a sophisticated Malvern nanosizer (Make: Nano ZS, Model: ZEN 3600). Subsequent to characterization, the synthesized nanoparticles were dispersed in deionized water and subjected

to sonication for a period of 15 minutes to ensure homogeneity. The resulting particle size distribution was determined utilizing a refractive index of 1.33. Finally, the WO_3/C electrocatalyst was meticulously prepared following a prescribed methodology delineated in Figure 3.1.

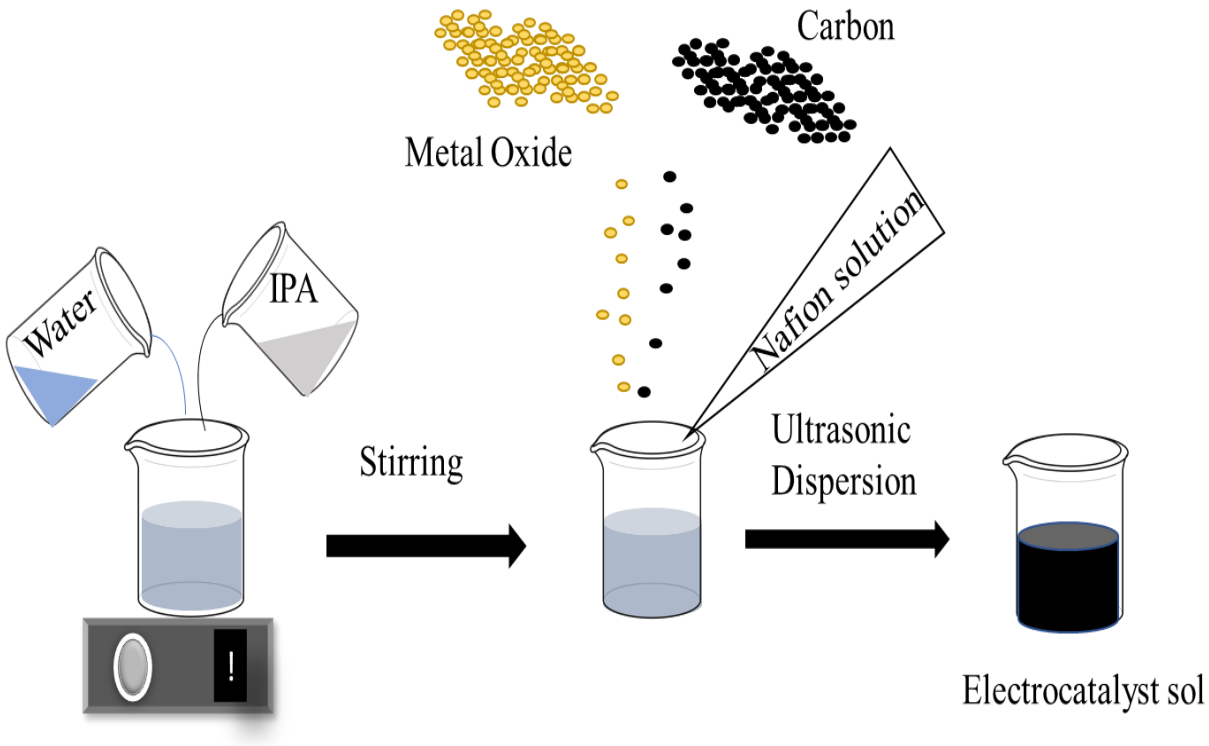

Figure 3.1 Schematic depiction for synthesizing the electrocatalyst sol using ultra-sound assisted sol-gel method

$$Na_2WO_4 + 2HCl \longrightarrow H_2WO_4 + 2NaCl \quad (1)$$

$$H_2WO_4 \longrightarrow WO_3 + H_2O \quad (2)$$

3.3 Physicochemical characterization

3.3.1 FESEM- EDAX

The morphology of the layered TiO_2@CNP and WO_3/C electrocatalysts coated on CP was observed by using FESEM & SEM. The samples were prepared by coating the synthesized sol on 1 cm × 1 cm carbon paper and dried for 12 h at room temperature. The sample was gold-sputtered to enhance the conductivity and loaded onto the sample holder. The surface

morphology of TiO_2@CNP electrocatalyst on CP was observed by SEM (Make: TESCAN ANALYTICS, Model: VEGA3). The elemental analysis was also carried out using EDX. The surface morphology of the synthesized WO_3/C electrocatalyst coated on carbon paper was observed using FESEM (model: Ultra 55, Make: Carl ZEISS). The topology of the bare carbon paper and electrocatalyst-coated carbon paper samples was observed.

3.3.2 FTIR

The chemical bonds present in the electrocatalysts were observed by using FTIR analysis. The sol of TiO_2@CNP, CNP, and WO_3/C was synthesized and layered on different glass slides and dried for 24 h at room temperature. The layers were peeled off after drying, and the powdered samples were further dried at 80°C for 2 h to remove the leftover traces of moisture. The powdered samples of TiO_2@CNP, CNP, WO_3/C, and WO_3 were blended with KBr and compressed to form pellets. Each sample was tested individually. The sample was securely placed into the sample holder of an FTIR (Make: PerkinElmer Spectrum, Model: 100S) and scanned over the wavenumber range from 400 to 4000 cm^{-1}.

3.3.4 XRD

XRD was used to identify the crystalline structure of TiO_2@CNP and WO_3/C electrocatalysts. The powdered TiO_2, TiO_2@CNP, CNP, and WO_3/C samples were dried at 60 °C for 3 h. Each sample was subjected to scanning separately. The sample was loaded onto an X-ray diffractometer (Make PANalytical, Model: X'Pert Powder). The spectrums were recorded with the diffraction angle (2θ) ranging from 10°–80° with a scan rate of 1° min^{-1}.

3.4 CV

CV tests were conducted using a Potentiostat/Galvanostat system (Make: Metrohm, Model: PGSTAT M204). The electrochemical cell employed in these experiments is a three-electrode

cell, having a platinum wire as the counter electrode and an Ag/AgCl electrode as the reference electrode shown in Figure 3.2. This setup was connected with PGSTAT.

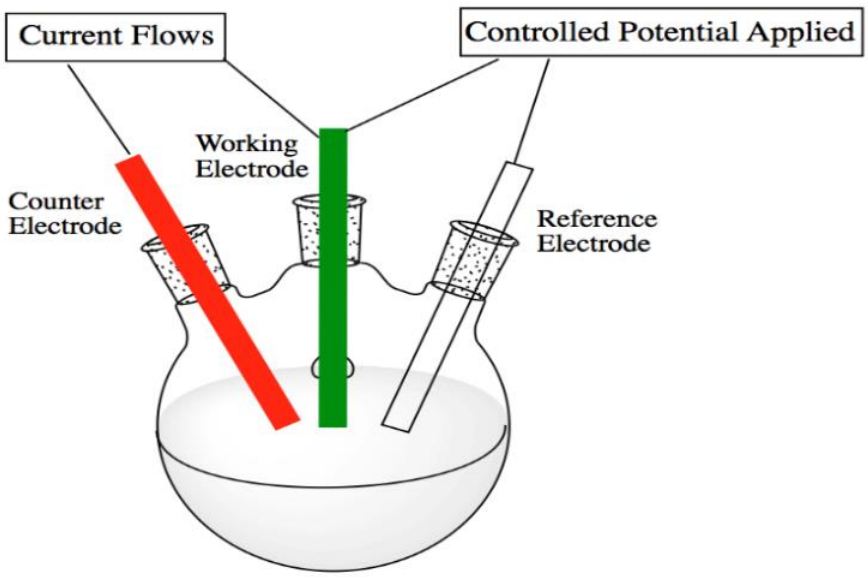

Figure 3.2. Schematic of three-electrode cell setup

CV of TiO_2@CNP: The TiO_2@CNP electrocatalyst has been developed and tested for its suitability in H_2-BQ RFB and HQ-BQ RFB. The electrochemical activity of the developed TiO_2@CNP electrocatalyst was assessed by CV analysis. The ratio of the powdered mixture (carbon + TiO_2) to Nafion was varied from 1:1 to 1:3 and 1:1 to 3:1 in the synthesized sol and recorded the voltammograms to find the optimal ratio. The sol with optimal composition was coated on 3 cm^2 carbon paper (TiO_2@CNP-CP) and tested in a 3-electrode cell with the electrolyte of 10 mM BQ in 0.5M H_2SO_4. The same study was repeated for the sol without TiO_2 to determine the enhanced activity of the TiO_2@CNP electrocatalyst comparatively.

CV of WO_3/C: The WO_3/C electrocatalyst has been developed for HQ-BQ RFB. The solubilities of HQ and BQ in H_2SO_4 were optimized for the RFB application (Bauer et al., 2020). The 1M, 2M, 3M, and 4 M sulfuric acid samples were prepared for the solubility test. To ascertain the solubility, 0.1 g of HQ was kept in four graduated glass bottles and labeled 1M

to 4M sulfuric acid. The sulfuric acid was added slowly to each corresponding bottle with the help of a micropipette, followed by sonication. The volume of the acid for the complete dissolution of 0.1g solid was determined. The same procedure was followed for the solubility study of BQ. The solubility was calculated based on the solute's weight and the volume of acid added (g/ml). This study was repeated four times, and the average has been taken as the solubility of HQ and BQ, respectively. The electrochemical activity of the synthesized WO_3/C electrocatalyst was determined by CV tests on PGSTAT. The electrocatalyst was coated on 3 cm^2 carbon paper and a glassy carbon electrode tip. The coated carbon paper (WO_3/C-CP) was used as working electrodes tested in a 3-electrode cell with the electrolyte of Hydroquinone in H_2SO_4. The above procedure was repeated by changing the working electrode to a coated glassy carbon electrode tip (WO_3/C-GC) and pristine carbon paper. Those mentioned above, all three working electrodes were also tested in Benzoquinone in H_2SO_4 electrolyte.

The CV data was used to obtain the enhanced electrochemical activity by the Tafel analysis. For Tafel analysis, the overpotential Vs logarithmic current density was plotted and fitted by linear equation 3.1.

$$\eta = a + b \log j \ldots\ldots\ldots\ldots (3.1)$$

where,

a = Intercept; b =Slope of the linear fit Tafel plot; j = Current density.

The catalyst performance is further assessed by finding electrochemically active surface area (ECSA) and Turnover frequency (TOF). For calculation of ECSA in positive half-cells of H_2-BQ RFB and both half-cells of HQ-BQ RFB. The CV tests at different scan rates were carried out by using TiO_2@CNP-CP, CNP-CP, WO_3/C-CP and CP electrodes as working electrode. The current values were read in a non-faradaic region at 0.2 V, plotted against the scan rate, and double-layer capacitance (C_{dl}) values were obtained. The ECSA was determined using equations 3.2 (Nayak et al., 2017; Tong et al., 2019; Yang et al., 2019).

$$ECSA = \frac{C_{dl}}{C_s} \ldots\ldots\ldots\ldots\ldots\ldots\ldots\ldots (3.2)$$

$$C_s = \frac{Area\ under\ the\ CV\ curve}{2 \times Area\ of\ electrode\ \times v \times \Delta V} \ldots\ldots\ldots\ldots\ldots\ldots (3.3)$$

Where,

C_{dl}= Double layer capacitance

Cs =Specific capacitance (standard carbon electrode)

v = Scan rate

ΔV= Potential range

TOF was calculated assuming every active site was accessible to the electrolyte (Tong et al., 2019; Yu et al., 2018). The TOF was determined using equation 3.4.

$$TOF = \frac{I}{2Fn} \quad \ldots\ldots\ldots\ldots\ldots (3.4)$$

Where,

I= Current (A = coulomb/s),

F = Faraday's constant (coulomb/mol),

n = Number of active sites (mol).

Factor ½ is since two electrons are transferred in the electrochemical reaction (Yin et al., 2021). The number of active sites was determined using CV at 100 mV s^{-1} scan rate. Assuming one electron transfer process for both reduction and oxidation, we can get the upper limit of the number of active sites (n) using equation 3.5.

$$n = \frac{\int_{V_1}^{V_2} I\Delta V}{2vF} \quad \ldots\ldots\ldots (3.5)$$

3.5 Single-cell charge-discharge

H_2-BQ RFB – Positive side: In the conducted experiments for half-cell charge discharge ((Figueredo-Rodríguez et al., 2017; Yourey et al., 2019), the electrochemical setup featured a three-electrode cell, incorporating a platinum wire as the counter electrode and an Ag/AgCl electrode as the reference electrode, as visually presented in Figure 3.3. This configuration was then connected to a PGSTAT instrument.

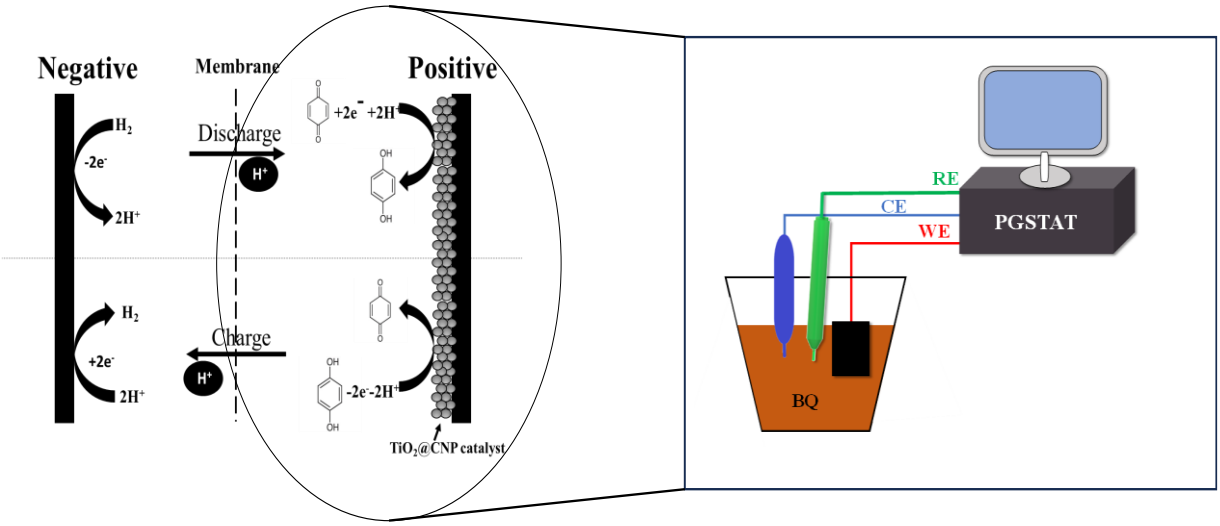

Figure 3.3. Schematic of experimental setup for half-cell charge discharge test

The sol with optimal composition was coated on 3 cm^2 carbon paper (TiO_2@CNP-CP) and tested in a 3-electrode cell with the electrolyte of 10 mM BQ in 0.5M H_2SO_4. Charge-discharge profiles were obtained, setting a lower cutoff at 0.1V and an upper limit at 0.8V. A controlled series of 50 charge-discharge cycles ensued, employing a constant current of 5mA at room temperature and atmospheric pressure. Following these procedures, the cell's efficiency was calculated, allowing for a comparative assessment with the baseline pristine carbon paper.

HQ-BQ RFB: The performance of the TiO_2@CNP and WO_3/C electrocatalysts was assessed by galvanic charge-discharge in HQ-BQ RFB. The flow cell with a 4 cm^2 active area was connected to PGSTAT, and the charge-discharge test was performed by employing TiO_2@CNP-CP, CNP-CP, WO_3/C-CP and CP electrodes. The graphite bipolar plates consist

of a serpentine flow field, copper plates were used as current collectors, and the Nafion117 membrane was used as a separator.

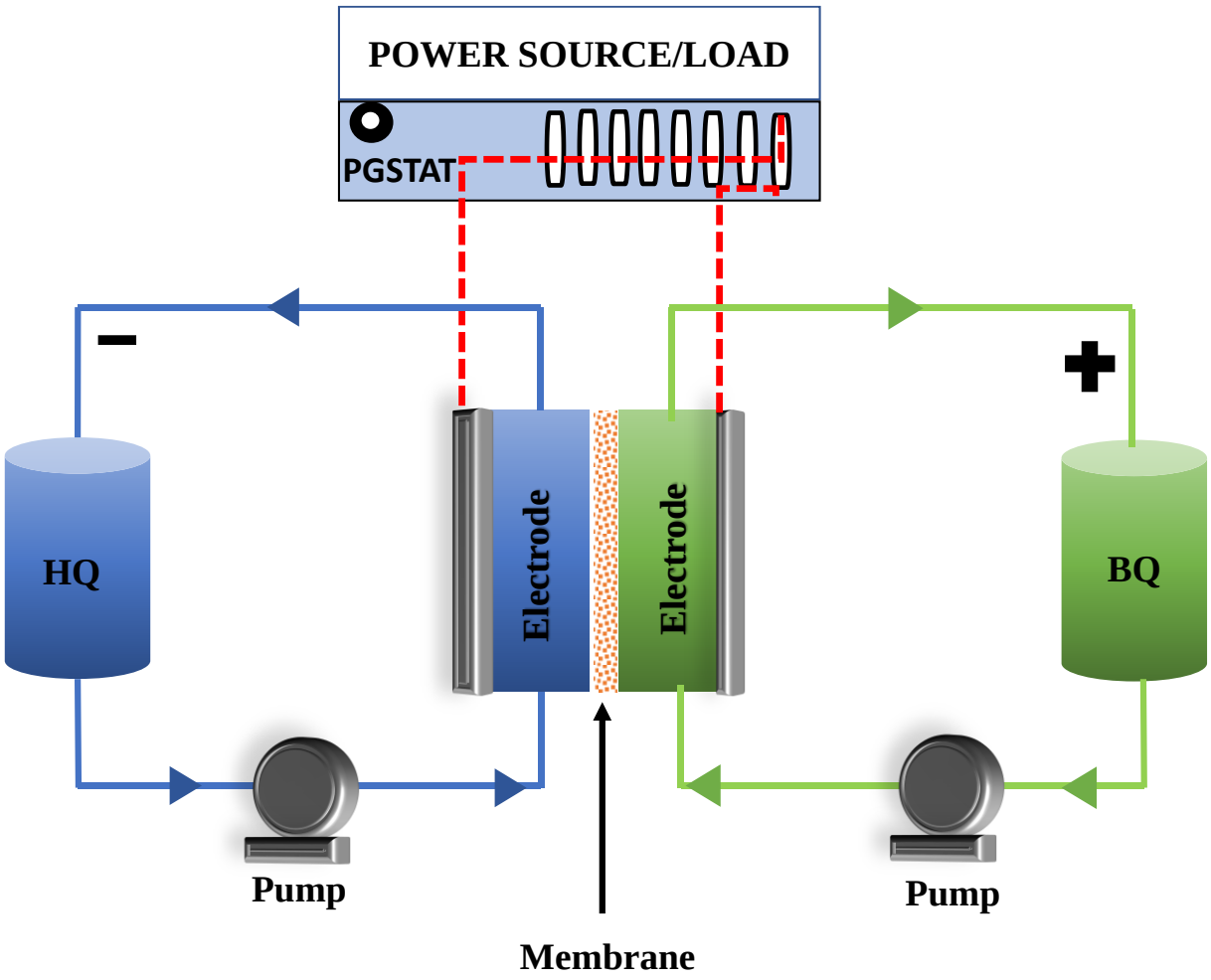

Figure 3.4. Schematic of HQ-BQ full cell setup for charge-discharge test

The 0.17M HQ and 0.18M BQ in 3M H_2SO_4 were used as anolyte and catholyte, respectively. The diaphragm pumps (Make: KnF & Model: Simdos 10) were employed to pump the electrolyte solutions into the cell. The 50 charge-discharge cyclic tests were performed with a constant current of 40 mA. The cutoff voltage limits of 1.2V and 0.2V are applied during charge and discharge, respectively. Keeping all the above conditions the same, the galvanostatic cyclic charge-discharge test was reconducted using pristine carbon paper, and the results were compared.

References

Bauer, S., Namyslo, J. C., Kaufmann, D. E., & Turek, T. (2020). Evaluation of Options and limits of Aqueous All-Quinone-Based Organic Redox Flow Batteries. Journal of The Electrochemical Society, 167(11), 110522.
https://doi.org/10.1149/1945-7111/aba338

H. A. Figueredo-Rodríguez, R. D. McKerracher, M. Insausti, A. Garcia Luis, C. Ponce de Leó, C. Alegre, V. Baglio, A. S. Aricò, & F. C. Walsh (2016). A Rechargeable, Aqueous Iron Air Battery with Nanostructured Electrodes Capable of High Energy Density Operation. Journal of The Electrochemical Society, 164 (6) A1148-A1157. https://iopscience.iop.org/article/10.1149/2.0711706jes

Joaquín de la Vega, Jordi-Roger Riba, & Juan Antonio Ortega-Redondo (2023). Real-Time Lithium Battery Aging Prediction Based on Capacity Estimation and Deep Learning Methods. Batteries,10(1), 10.
https://doi.org/10.3390/batteries10010010

Miu, E. V, McKone, J. R., & Mpourmpakis, G. (2022). The Sensitivity of Metal Oxide Electrocatalysis to Bulk Hydrogen Intercalation: Hydrogen Evolution on Tungsten Oxide. Journal of the American Chemical Society, 144(14), 6420–6433. https://doi.org/10.1021/jacs.2c00825

Nayak, A. K., Verma, M., Sohn, Y., Deshpande, P. A., & Pradhan, D. (2017). Highly active tungsten oxide nanoplate electrocatalysts for the hydrogen evolution reaction in acidic and near neutral electrolytes. ACS Omega, 2(10), 7039–7047. https://doi.org/10.1021/acsomega.7b01151

Patel, P. P., Jampani, P. H., Datta, M. K., Velikokhatnyi, O. I., Hong, D., Poston, J. A., Manivannan, A., & Kumta, P. N. (2015). WO3 based solid solution oxide - Promising proton exchange membrane fuel cell anode electrocatalyst. Journal of Materials Chemistry A, 3(35), 18296–18309.
https://doi.org/10.1039/c5ta03792a

Tong, J., Li, Y., Bo, L., Li, W., Li, T., Zhang, Q., Kong, D., Wang, H., & Li, C. (2019). CoP/N-Doped Carbon Hollow Spheres Anchored on Electrospinning Core–Shell N-Doped Carbon Nanofibers as Efficient Electrocatalysts for Water Splitting. ACS Sustainable Chemistry & Engineering, 7(20), 17432–17442.
https://doi.org/10.1021/acssuschemeng.9b04643

Yang, F., Huang, S., Zhang, B., Hou, L., Ding, Y., Bao, W., Xu, C., Yang, W., & Li, Y. (2019). Facile Synthesis of Well-Dispersed Ni2P on N-Doped Nanomesh Carbon Matrix as a High-Efficiency Electrocatalyst for Alkaline Hydrogen Evolution Reaction. In Nanomaterials (Vol. 9, Issue 7).
https://doi.org/10.3390/nano9071022

Yin, Q., Xu, Z., Lian, T., Musaev, D. G., Hill, C. L., & Geletii, Y. V. (2021). Tafel slope analyses for homogeneous catalytic reactions. Catalysts, 11(1), 1–11. https://doi.org/10.3390/catal11010087

CHAPTER 4

TiO_2@CNP ELECTROCATALYST FOR H_2-BQ RFB

Chapter 4

TiO_2@CNP Electrocatalyst for H_2-BQ RFB

The experimental part of the TiO_2@CNP electrocatalyst synthesis and its applicability within the positive half-cell of the H_2-BQ Redox Flow Battery (RFB) is discussed in chapter 3. This chapter details the analysis of synthesis process of TiO_2@CNP, outlining the procedures used to fabricate this critical component.

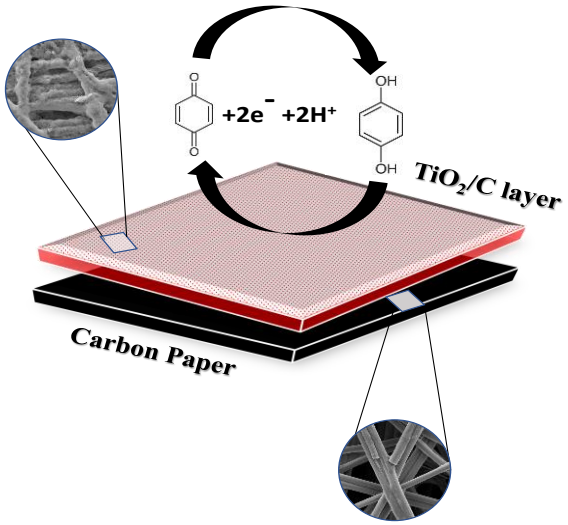

Figure 4.1 Schematic of the application of developed electrocatalyst

Following synthesis, the electrocatalyst undergoes rigorous characterization using various analytical techniques such as FESEM, FTIR, XRD, and CV to assess its structural and electrochemical properties. The performance of the H_2-BQ RFB cell incorporating the TiO_2@CNP electrocatalyst is evaluated through CV and GCD tests, providing insights into parameters like coulombic efficiency, voltage efficiency, and energy efficiency. Through a systematic analysis of synthesis, characterization, and performance evaluation, this study aims to elucidate the role of TiO_2@CNP in enhancing the efficiency and performance of RFB systems, contributing to the development of sustainable energy storage solutions. Figure 4.1 shows the overview of schematic of the application of developed electrocatalyst

4.1 Experimental

The detailed explanation of experimental procedure of synthesis of TiO_2@CNP electrocatalyst, physicochemical characterization, electrochemical and characterization and charge-discharge test of positive side of H_2-BQ RFB are illustrated in sections 3.3, 3.4 and 3.5 respectively. The results of these characterization studies of the catalyst are analyzed for its suitability in H_2-BQ RFB and presented in the subsequent section.

4.2 Results and discussion

4.2.1 SEM-EDAX

The SEM images of CP and TiO_2@CNP–CP samples were captured for analysis. The surface morphology of CP and TiO_2@CNP–CP are shown in Figures. 4.2a and 4.2b. It is observed that the bare carbon paper in Figure 4.2a has smooth fibers with large pores. The same was drop coated with synthesized TiO_2@CNP electrocatalyst and the smooth fibers have become rough with the increased surface area as shown in Figure. 4b. EDX was also carried out for the same sample and obtained spectra shown in Figure 4.2c. The main elemental peaks observed were Ti, C, F, and O which confirms the presence of material that was used for synthesis. The relative

weight percentile of C, F, Ti, and O are 96.66, 0.17, 0.06, and 3.17 respectively. The detectable amount of impurity is not observed in the sample. EDX analysis indicates successful preparation of TiO_2@CNP.

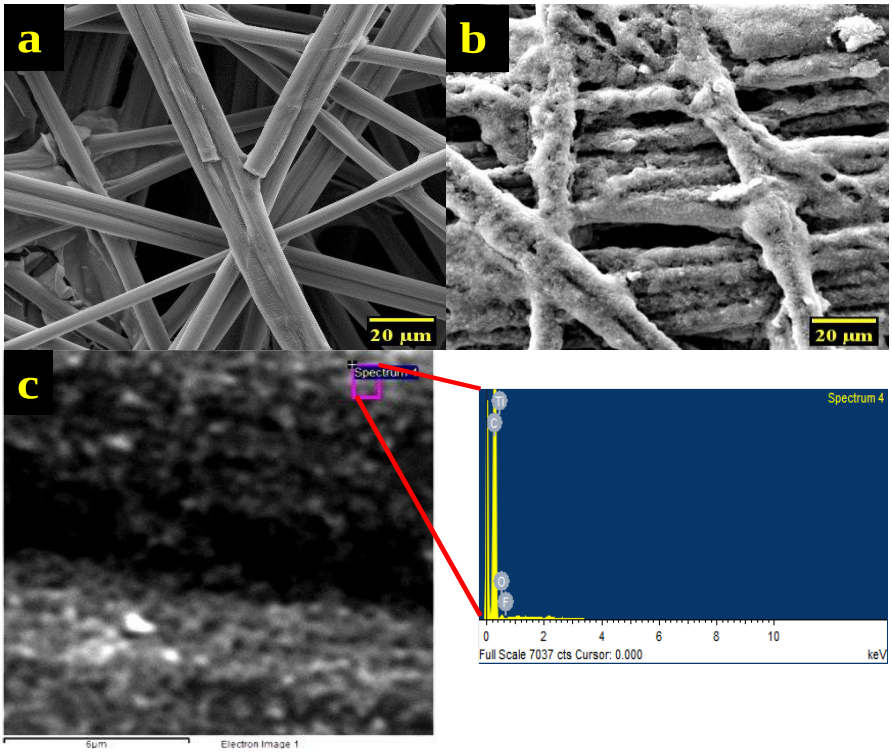

Figure 4.2 SEM images of (a) CP (b) TiO_2@CNP-CP (c) EDAX spectra of TiO_2@CNP-CP

4.2.2 FTIR

The functional groups were identified by FTIR spectroscopy. The spectra of synthesized TiO_2@CNP electrocatalyst and CNP are shown in Figure 4.3. The identified peaks and their assigned bonds are summarized in Table 4.1. The metal oxides can form weaker and wider peaks at a low wavelength. The peaks at 1731 cm^{-1} and 1452 cm^{-1} are attributed to the bending vibrations Ti–OH band and TiO_2 bond vibrations respectively (Foratirad et al., 2017). The bonds at 517 cm^{-1} and 668 cm^{-1} are associated with Ti–C (Ogunlana et al., 2023) and O–Ti–O (Abdulsada et al., 2018) stretching respectively and indicate the interaction between TiO_2 particles and carbon particles. The above peaks indicate the presence of TiO_2 in the TiO_2@CNP electrocatalyst and were absent in the spectra of CNP. The peaks at around 3390 cm^{-1}, 2920

cm^{-1}, 1620 cm^{-1}, 1230 cm^{-1} and 1155 cm^{-1} are assigned to –OH stretching, CH_2 stretching, H_2O band, C–OH stretching, and C–O–C stretching respectively (Loekitowati Hariani et al., 2018) are found common in both the samples as shown in Figure 4.3. The identified peaks confirm the successful preparation of the electrocatalyst. The additional peaks are also responsible for the defects available on the active surface of the electrode which gives an improved electrochemical performance.

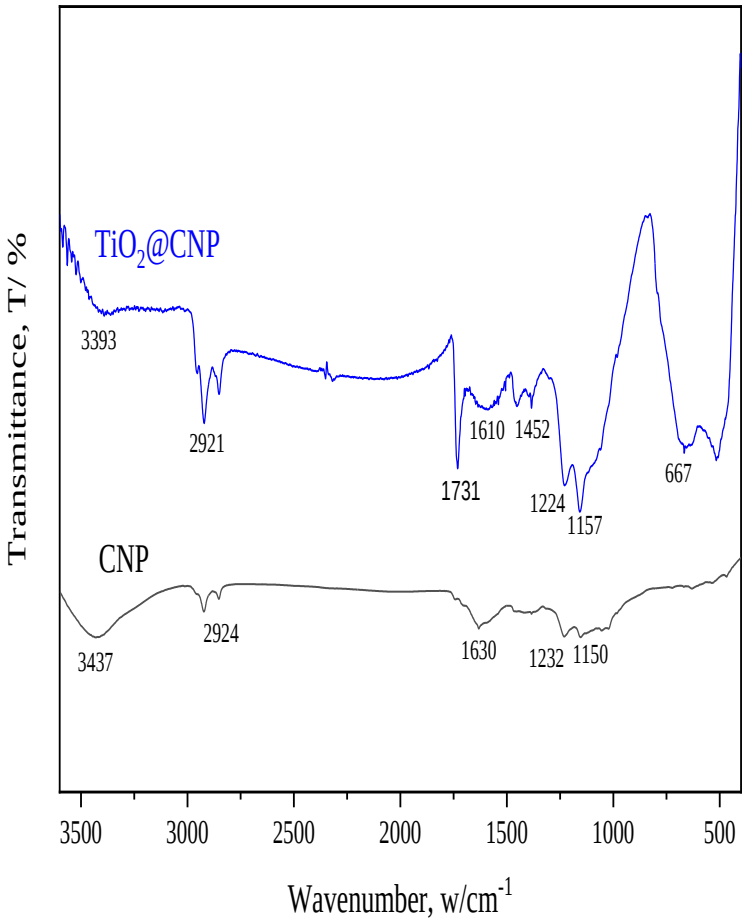

Figure 4.3 FTIR spectrum of the TiO_2@CNP, CNP

Table 4.1. Identified functional bonds for the CNP and TiO_2@CNP

Electro catalyst	**IR band (cm^{-1})**	**Assignment**
CNP	3434	-OH Stretching
	2924	-CH_2 Stretching
	1630	-H_2O band
	1232	-C-OH Stretching
	1150	-C-O-C Stretching
TiO_2@CNP	3393	-OH Stretching
	2921	-CH_2 Stretching
	1731	Ti-OH bending vibration
	1610	-H_2O band
	1452	TiO_2 lattice vibration
	1234	-C-OH Stretching
	1157	-C-O-C Stretching
	667	O-Ti-O Stretching
	517	Ti-C Stretching

4.2.3 XRD

The diffractograms of powdered TiO_2@CNP, TiO_2 and CNP samples are shown in the Figure 4.4. The peaks indexed to (101), (110), (103), (004), (112), (200), (105), (211), (204), (116) and (215) confirms the crystalline nature of TiO_2 and suggested the tetragonal structure

of combination of anatase and rutile phase of TiO_2 (Chen et al., 2006). The characteristic diffraction peaks at 2θ = 25.2° (101), 37.87° (004), 48.13° (200), 62.9° (204), 68.8° (116), 75.11° (215) confirm the presence of anatase phase and the peaks at 2θ = 26.4° (110), 36.9° (103), 39.5° (112), 53.9° (105), 55° (211) confirm the presence rutile phase of TiO_2. Further, two broad peaks centered at 2θ = 26.4° and at 44.7° of CNP confirm the amorphous nature of the activated carbon (Rahim et al., 2015). The XRD spectrum of TiO_2@CNP shows both the characteristic peaks of TiO_2 and CNP. The TiO_2@CNP is found to be partially crystalline which can be an attributable factor for improved electrocatalytic activity (Jiang et al., 2017).

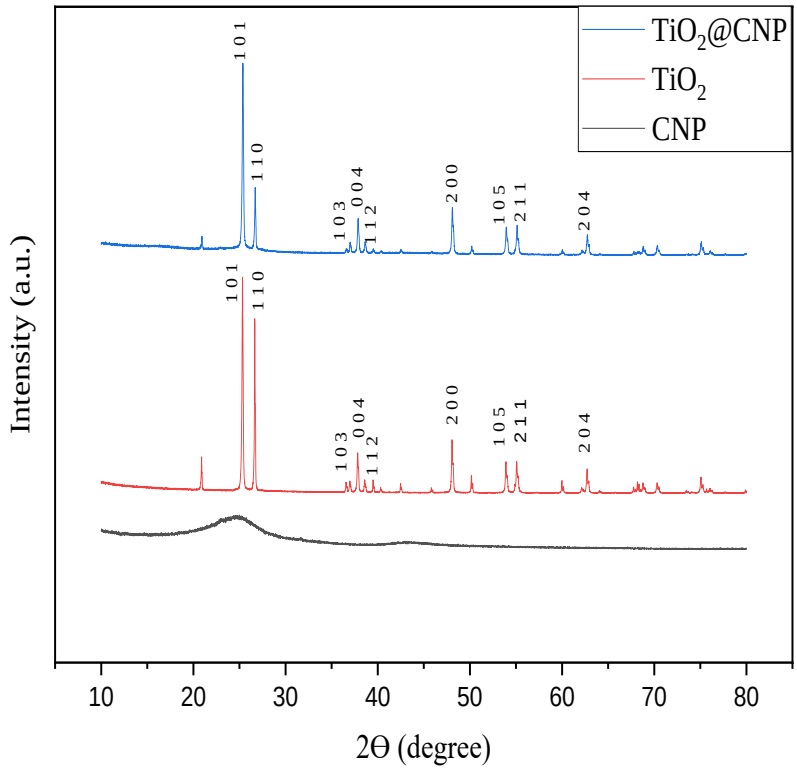

Figure 4.4 X-Ray diffractogram of the TiO_2@CNP, TiO_2 and CNP

4.2.4 Cyclic Voltammetry (CV)

The electro-chemical performance of the synthesized TiO_2@CNP catalyst was assessed by CV. The ratio of (TiO_2+CNP) to Nafion was varied from 1:1 to 1:3 and 1:1 to 3:1 in the synthesized electrocatalyst and voltammograms were obtained (Figure 4.5). It was observed that the ratio of 1:3 has delivered duck-shaped voltammogram with peaks of similar magnitude on both the forward and reverse scans indicated the more reversibility of redox reaction (Venton & Cao, 2020; Wang et al., 2014). Hence, further studies were carried out with the optimal (TiO_2+CNP) to Nafion ratio of 1:3. The CV was conducted for TiO_2@CNP coated on CP (TiO_2@CNP - CP), CNP-CP and CP shown in Figure 4.6. The TiO_2@CNP has given an enhanced current density (5.4 mA cm^{-2}). This can be attributed to higher catalytic activity with enhanced active surface area of TiO_2@CNP-CP. Further, it is also confirmed by calculating the ECSA using equation 3.2. The CV tests at different scan rates were carried out by using TiO_2@CNP-CP, CNP-CP and CP electrodes. The current values were read in non-faradaic region at 0.2 V, plotted against the scan rate and obtained the values of C_{dl} as shown Figure 4.7.

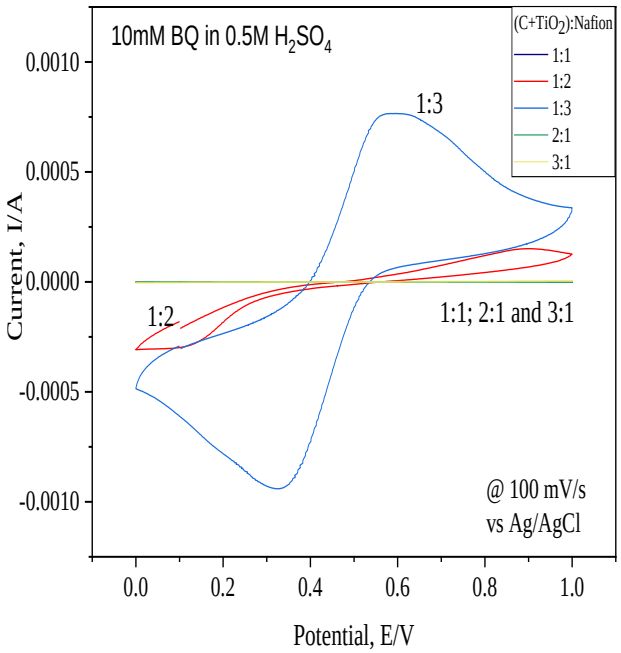

Figure 4.5 CV curves for the varied ratio of (TiO_2+C) to Nafion

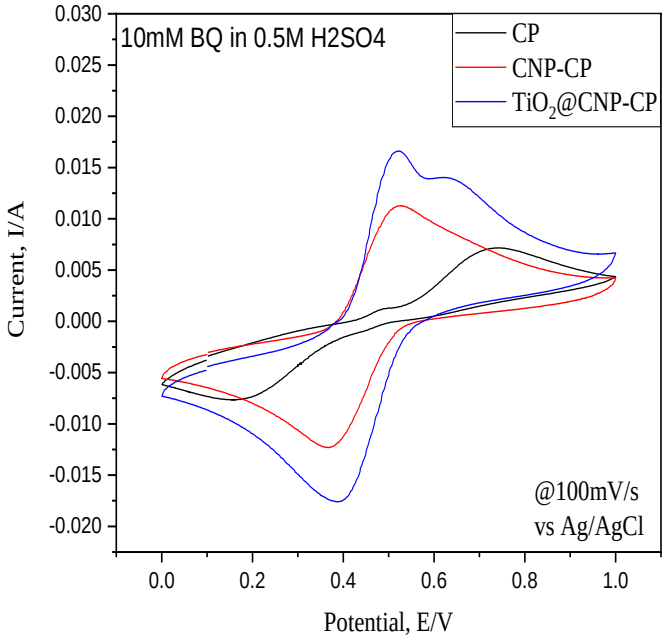

Figure 4.6 The electro-catalytic activity of CP, CNP-CP and TiO_2@CNP-CP

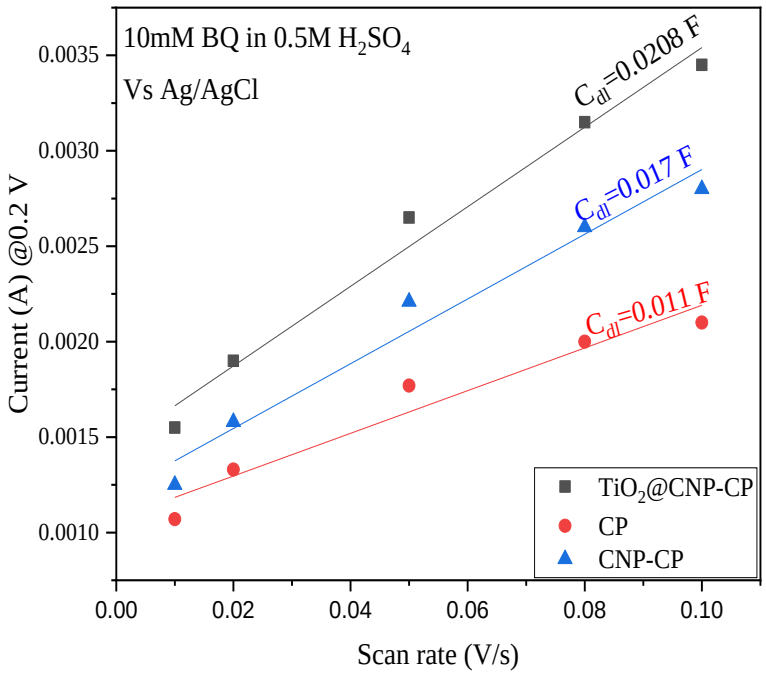

Figure 4.7 Electrochemical double layer capacitance (C_{dl}) of CP, CNP-CP, and TiO_2@CNP-CP

The specific capacitance (Cs) was calculated using standard carbon paper electrode in 10 mM BQ in 0.5M H_2SO_4 and found out to be 0.0025 F/cm^2. The determined ECSAs of TiO_2@CNP-CP, CNP-CP, and CP are 8.32 cm^2, 6.8 cm^2 and 4.4 cm^2 respectively. The TiO_2@CNP-CP electrode has higher ECSA and provides higher specific catalytic activity comparatively. The peak current values were scaled to ECSA and summarized in Table 4.2.

Table 4.2. Summary of the ECSA and scaled peak current densities of CP, CNP-CP and TiO_2@CNP-CP

Sample	**TiO_2@CNP-CP**	**CNP-CP**	**CP**
ECSA (cm^2)	8.32	6.8	4.4
$i_{pa\ (A)}$	0.016	0.011	0.007
$i_{pc\ (A)}$	0.017	0.012	0.007
$i_{pa\_scaled\ (mA/cm^2)}$	1.92	1.61	1.590
$i_{pc\_scaled\ (mA/cm^2)}$	2.04	1.764	1.590

The TiO_2@CNP-CP displayed the highest anodic peak current of 0.016 A and maximum cathodic peak current of −0.017 A with a least peak separation distance of 138 mV. The lower peak separation inferred that the developed electrocatalyst gives high reversibility to the redox reaction in the positive half-cell of H_2-BQ RFB. The TOF & number of active sites were calculated for TiO_2@CNP and CNP electrocatalysts using the equation 3.3 and equation 3.4. The calculated number of active sites of TiO_2@CNP-CP, CNP-CP and CP electrodes are 4.7105 × 10^{-6} mol, 3.2440 × 10^{-6} mol, and 1.5235 × 10^{-6} mol respectively. The corresponding TOF of TiO_2@CNP-CP, CNP-CP and CP electrodes were calculated at 0.5 V are 0.0173 s^{-1}, 0.0169 s^{-1} and 0.0034 s^{-1} respectively. The TiO_2@CNP-CP with higher TOF value possesses the

improved catalytic activity. Figure 4.8 shows the Tafel plots, the overpotential Vs logarithmic current density and fitted by linear equation 3.1, The Tafel slopes of CP, CNP-CP, and TiO_2@CNP-CP are 121.8 mV, 54 mV, and 18 mV respectively.

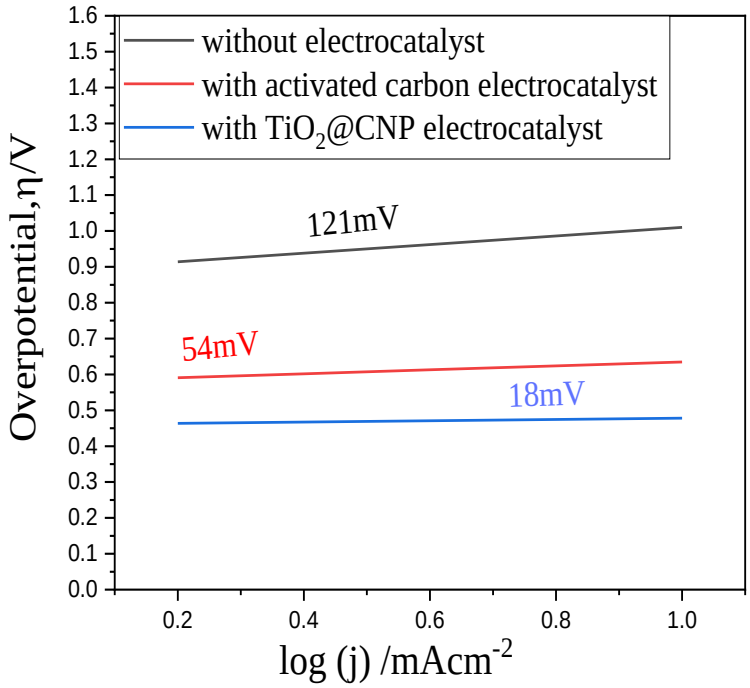

Figure 4.8 Tafel Plots CP, CNP-CP and TiO_2@CNP-CP

The lower slope of the TiO_2@CNP-CP suggests that the minimum overpotential is required to produce the higher current which implies the enhanced reaction kinetics. The CV curves with the TiO_2@CNP-CP were obtained at different scan rates. The system peak current is directly proportional to scan rate and suggests that the positive half-cell reaction of H_2-BQ RFB is surface reaction controlled.

4.3 Half-cell charge-discharge

The constant current charge-discharge test was conducted in a three-electrode cell assembly which resembles the positive half-cell of H_2-BQ RFB. The synthesized TiO_2@CNP electrocatalyst was drop-coated on carbon paper and used as the working electrode. The half-

cell is subjected to 50 cycles of charge-discharge at 1.6 mA cm^{-2} current density using CP and TiO_2@CNP-CP. The GCD of half-cell with TiO_2@CNP-CP has been shown in Figure 4.9 which shows the consistent cycles. Throughout the test, TiO_2@CNP-CP has shown the voltage efficiency of >74% and 99% coulombic efficiency. Coulombic efficiency is consistent and not fading with respect to the cycles. The energy efficiency of cell using synthesized TiO_2@CNP-CP is 73% while it is 55% with CP as shown in Figure 4.10. The maximum energy efficiency of quinone based batteries is nearly 66% (Mahanta et al., 2022; Pinheiro et al., 2023) reported, whereas the cell with TiO_2@CNP-CP electrode delivered the 73% energy efficiency.

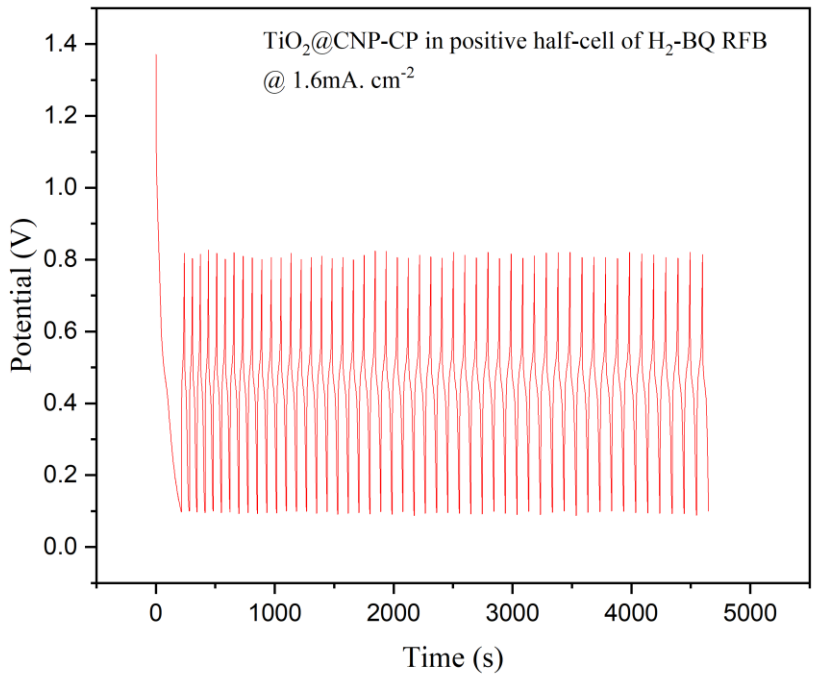

Figure 4.9. Half-cell charge-discharge cycles of TiO_2@CNP-CP in positive half-cell of H_2-BQ RFB

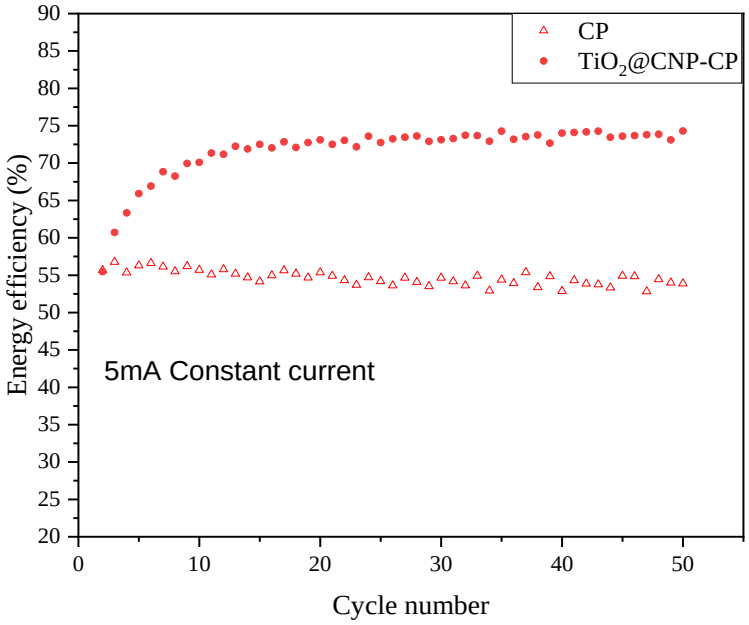

Figure 4.10. Energy efficiency of H_2-BQ RFB positive half-cell with CP and TiO_2@CNP-CP

4.4 Conclusion

The TiO_2@CNP electrocatalyst was successfully synthesized for the positive half-cell of H_2-BQ RFB. The TiO_2@CNP electrocatalyst sol was synthesized by the ultrasound dispersion method. It was coated on carbon paper using the drop coating method. The surface morphology of coated carbon paper was analyzed by SEM and observed the presence of rougher fibers on the surface. FTIR confirms the functional bonds of $TiO_2$and carbon interaction. XRD analysis shows the formation of semi crystalline TiO_2@CNP with anatase and rutile phases. The TiO_2@CNP-CP has shown higher peak current densities (5.4 mA cm^{-2}), small peak separation, higher ECSA and TOF values which indicates higher reaction kinetics and reversibility. The synthesized TiO_2@CNP-CP gives the lower Tafel slope of 18.14 mV which signifies enhanced reaction kinetics. The performance of the electrocatalyst was tested in H_2-BQ RFB positive half-cell and subjected to 50 cycles of charge-discharge at 1.6 mA cm^{-2} current density. The cell delivers higher energy efficiency of 73% compared to pristine carbon paper and proves its suitability for the application in H_2-BQ RFB.

References

Abdulsada, A. H., Mishjil, K. A., & Abd, A. N. (2018). Effect of thermal annealing on properties of polycrystalline Titanium dioxide (TiO2) thin film prepared by simple chemical method. Journal of Physics: Conference Series, 1032(1), 12037. https://doi.org/10.1088/1742-6596/1032/1/012037

Attar, A. S., Ghamsari, M. S., Hajiesmaeilbaigi, F., Mirdamadi, S., Katagiri, K., & Koumoto, K. (2008). Synthesis and characterization of anatase and rutile TiO2 nanorods by template-assisted method. Journal of Materials Science, 43(17), 5924–5929. https://doi.org/10.1007/s10853-008-2872-y

Calvo, M. E., Candal, R. J., & Bilmes, S. A. (2001). Photooxidation of Organic Mixtures on Biased TiO2 Films. Environmental Science & Technology, 35(20), 4132–4138. https://doi.org/10.1021/es010613r

Chen, M. L., Bae, J. S., & Oh, W. C. (2006). Characterization of AC/TiO2 composite prepared with pitch binder and their photocatalytic activity. Bulletin of the Korean Chemical Society, 27(9), 1423–1428. https://doi.org/10.5012/bkcs.2006.27.9.1423

Foratirad, H., Baharvandi, H. R., & Maragheh, M. G. (2017). Chemo-rheological behavior of aqueous titanium carbide suspension and evaluation of the gelcasted green body properties. Materials Research, 20(1), 175–182. https://doi.org/10.1590/1980-5373-MR-2016-0410

Jiang, W.-J., Niu, S., Tang, T., Zhang, Q.-H., Liu, X.-Z., Zhang, Y., Chen, Y.-Y., Li, J.-H., Gu, L., Wan, L.-J., & Hu, J.-S. (2017). Crystallinity-Modulated Electrocatalytic Activity of a Nickel(II) Borate Thin Layer on Ni3B for Efficient Water Oxidation. Angewandte Chemie, 129(23), 6672–6677. https://doi.org/10.1002/ange.201703183

Loekitowati Hariani, P., Muryati, & Fatma, F. (2018). Synthesis Alumina-Activated Carbon Composite Using Sol-Gel Method As Adsorption for Methylene Blue Dye. Journal of Physics: Conference Series, 1095(1). https://doi.org/10.1088/1742-6596/1095/1/012026

Mahanta, V., Gupta, R., & Ramanujam, K. (2022). Hydrobromide Salt of Tribromodopamine as a Positive Electroactive Species with a Three-Electron Redox Process for Redox Flow Battery Applications. ACS Applied Energy Materials, 5(12), 15166–15174. https://doi.org/10.1021/acsaem.2c02833

Ogunlana, M. O., Muchie, M., Oladijo, O. P., & Erinosho, M. (2023). Effect of Microstructural and Tribological Behaviors of Sputtered Titanium Carbide Thin Film on Copper Substrate. Materials, 16(1). https://doi.org/10.3390/ma16010174

Pinheiro, D., Sousa, J. F. M., Pineiro, M., Valente, A. J. M., & Seixas de Melo, J. S. (2023). Non-pre-treated sulfonated poly(ether ether ketone) membrane as an efficient alternative for Nafion in acidic aqueous organic redox flow batteries. Journal of Energy Storage, 57, 106201. https://doi.org/10.1016/j.est.2022.106201

Venton, B. J., & Cao, Q. (2020). Fundamentals of fast-scan cyclic voltammetry for dopamine detection. Analyst, 145(4), 1158–1168.
https://doi.org/10.1039/C9AN01586H

Wang, W., Fan, X., Liu, J., Yan, C., & Zeng, C. (2014). A novel mechanism for the oxidation reaction of VO2+ on a graphite electrode in acidic solutions. Journal of Power Sources, 261, 212–220.
https://doi.org/10.1016/j.jpowsour.2014.03.053

CHAPTER 5

WO_3/C ELECTROCATALYST FOR HQ-BQ RFB

Chapter 5

WO_3/C Electrocatalyst for HQ-BQ RFB

This chapter presents a comprehensive exploration into the analysis of synthesis and characterization of the WO_3/C electrocatalyst, coupled with an in-depth assessment of its performance within the context of full-cell HQ-BQ RFBs. The analysis delves into meticulous detail, encompassing a range of sophisticated analytical techniques such as FESEM, FTIR, XRD, and CV. These methodologies afford a nuanced understanding of the electrocatalyst's structural composition, surface morphology, and chemical properties. Moreover, the effectiveness of the RFBs is rigorously evaluated through GCD testing, offering crucial insights into their electrochemical performance, energy efficiency, and overall operational viability. The performance of the cell with WO_3/C electrocatalyst is assessed by charge discharge test and presented. and its suitability in the HQ-BQ RFB. Through this multifaceted approach, a comprehensive picture emerges, elucidating both the fundamental characteristics of the electrocatalyst and its practical utility within redox flow battery applications.

5.1 Experimental

The detailed explanation of experimental procedure of synthesis of WO_3/C electrocatalyst, physicochemical characterization, electrochemical and characterization and charge-discharge test of positive side of HQ-BQ RFB are illustrated in sections 3.3, 3.4 and 3.5 respectively. The results of these characterization studies of the catalyst are analyzed for its suitability in HQ-BQ RFB and presented in the subsequent section.

5.2 Results and discussion

5.2.1 Synthesis of WO_3/C

Following the procedure described in section 3.2, the WO_3 nanoparticle were synthesized and the synthesis timeline image is shown in Figure 5.1. The precursor slurry is shown in Figure 5.1 (a) presents the, which undergoes vacuum filtration and the filtered H_2WO_4 cake has been obtained as shown in Figure 5.1 (b). The cake was dried and the H_2WO_4 particles were collected and shown in Figure 5.1 (c). These dried particles were calcinated in tubular furnace at 350°C to obtain WO_3 particles. The average particle size of the synthesized WO_3 particles was found to be 422 nm by using the DLS technique.

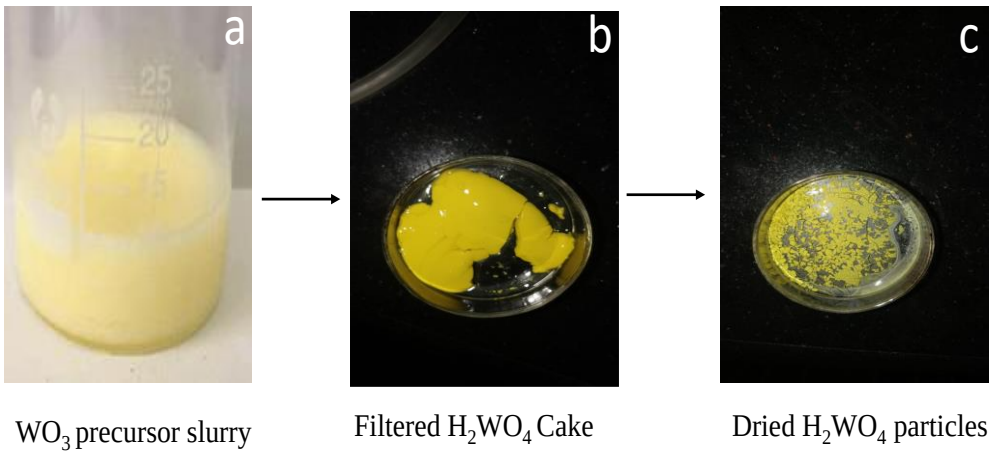

Figure 5.1 Synthesis timeline of WO_3 Particles

5.2.2 FESEM

The surface morphology of WO_3/C electrocatalyst layered carbon paper was observed by FESEM. The images of carbon paper and WO_3/C electrocatalyst layered carbon paper are shown in Figure 5.2a and Figure 5.2b respectively. The carbon paper (Figure 5.2a) has smooth fiber structure and contains very fewer active sites. The roughness of the surface is increased after the coating of the developed WO_3/C electrocatalyst. There are more active sites available on the surface as shown in Figure 5.2b.

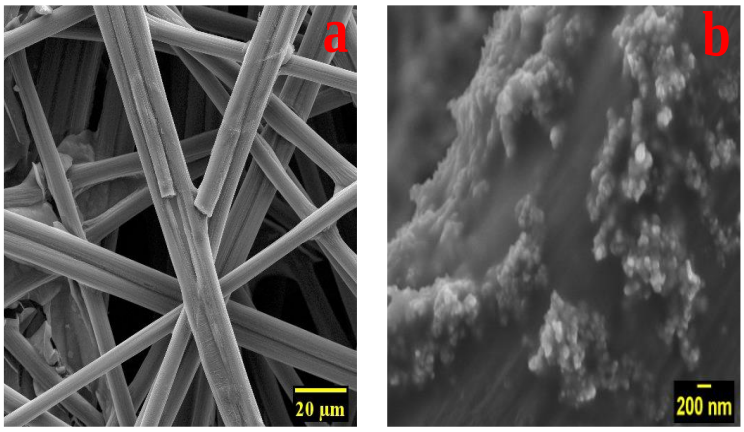

Figure 5.2. FESEM images of (a) carbon paper, (b) WO_3/C electrocatalyst carbon paper

5.2.3 XRD

The diffractograms of activated carbon and WO_3/C are shown in Figure 5.3. The diffractogram of activated carbon shows the amorphous nature. The sharp peaks of WO_3/C electrocatalyst represent its crystalline nature. The characteristic diffraction peaks are identified at 2Θ angle of 23°, 24°, 29°, 33.62°, 34.03°, 41.42° and 55.42° which are in line with the peaks of orthorhombic crystal structure of WO_3 (Waring, 1966). These absolute crystalline peaks and the presence of the metal oxide is responsible for the enhanced electrochemical performance of the electrocatalyst (Jiang et al., 2017).

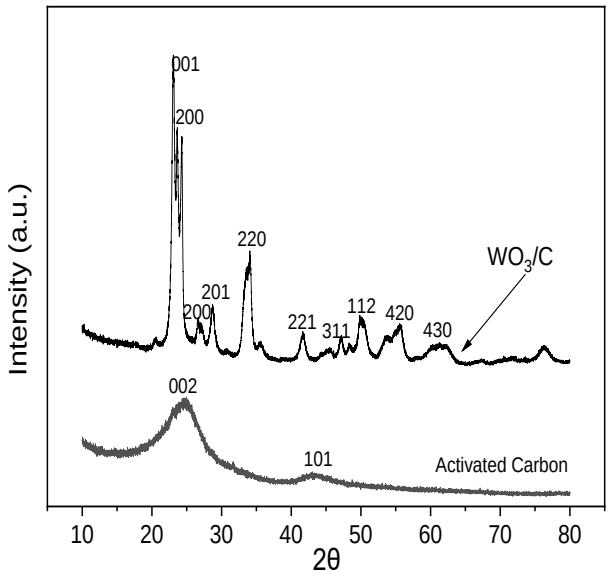

Figure 5.3. XRD diffractograms of WO_3/C and activated carbon

5.2.4 FTIR

The functional bonds of the developed WO_3/C electrocatalyst is shown in Figure 5.4 FTIR spectra of activated carbon and synthesized WO_3 are taken independently and compared. It was observed that all characteristic functional groups of mixed compounds are present in the WO_3/C electrocatalyst. The peaks at 3425 cm^{-1} and 1630 cm^{-1} represent the stretching vibration of the -OH group and H-O-H stretching respectively are found common which may be mapped to surface absorbed water molecules (Jothivenkatachalam et al., 2014). The -C-O-H stretching is observed at 966 cm^{-1} signifies presence of carbon. The peak at 727 cm^{-1} is corresponds to O-W-O bond shortening (Guéry et al., 1997). The peaks at 633 cm^{-1} and 1233 cm^{-1} characterization peaks are ascribed to the CF_2 group from the Nafion binder. The peak at 1059 cm^{-1} is attributed to W-C stretching and confirms the interaction of carbon and tungsten (Hoffmann et al., 2003). The assignment of functional bonds of the WO_3/C electrocatalyst are summarized in Table 5.1.

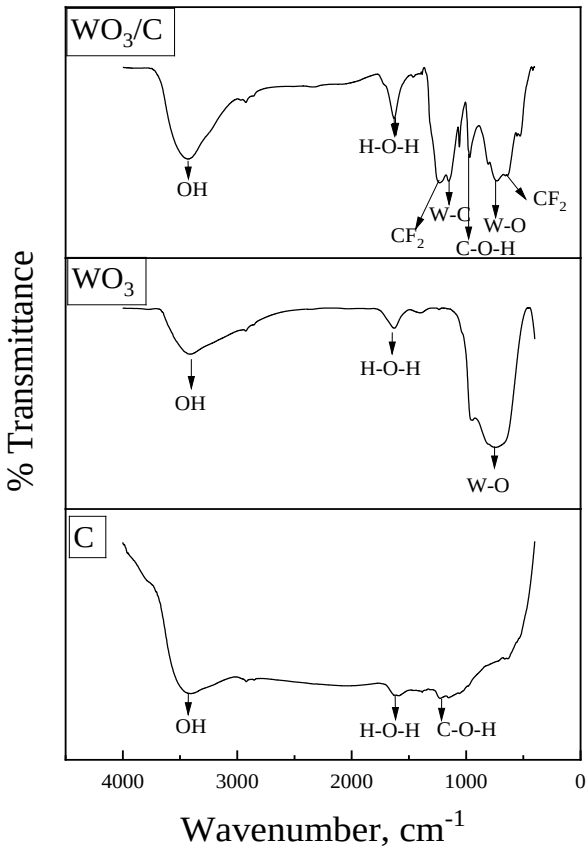

Figure 5.4. FTIR spectrum of WO_3/C, WO_3 and activated carbon

Table 5.1 Summary of identified functional bonds for the WO_3/C, WO_3, and activated carbon

Sr. No.	Wave number (cm^{-1})	Assignment
1.	633	-CF_2 Wagging
2	727	-W-O Shortening
3	966	-C-O-H Stretching
4	1059	W-C Stretching
5	1233	-CF_2 Stretching
6	1630	H-O-H Stretching
7	3425	O-H Stretching

5.2.5 Solubility test

The solubility of HQ and BQ in different concentrations of sulfuric acid were measured at room temperature (30ºC) shown in Figure 5.5.

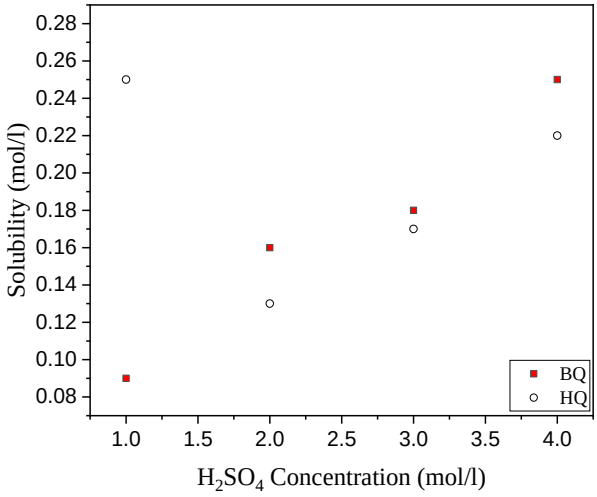

Figure 5.5. Solubilities of Hydroquinone and 1,4 P-Benzoquinone in sulfuric acid

It was observed that the solubility of BQ in H_2SO_4 was limiting and increases with increasing sulfuric acid concentration. To prevent the battery system from osmotically driven flux the concentration of supporting electrolyte (H_2SO_4) must be the same in both the half-cells of the battery (Kushner et al., 2020). Therefore, 3M H_2SO_4 solution has been chosen as the supporting electrolyte for this battery system. The solubilities of HQ and BQ in 3M H_2SO_4 were determined as 0.17 mol/l and 0.18 mol/l respectively and these concentrations were used for CV and charge-discharge tests.

5.2.6 CV

The electrocatalytic activity of developed WO_3/C electrocatalyst in negative half-cell which consist of 0.17 M HQ in 3M H_2SO_4 is assessed by cyclic voltammetry test. The cyclic voltammograms of GC and WO_3/C-GC are shown in Figure 5.6(a) and compared. The detailed parameter values of CV are summarized in Table 5.2. The peak current values I_{pa} & I_{pc} of WO_3/C-GC are higher and peak separation is lower than that of the GC. It is evident that the

developed WO_3/C-GC has given an enhanced current density compared to the GC electrode. The ratio of anodic to cathodic peak current is also closer to unity which concludes that the system is more reversible for WO_3/C electrocatalyst (Jeong et al., 2013). The similar performance of WO_3/C is observed in positive half-cell as well is shown in Figure 5.6b.

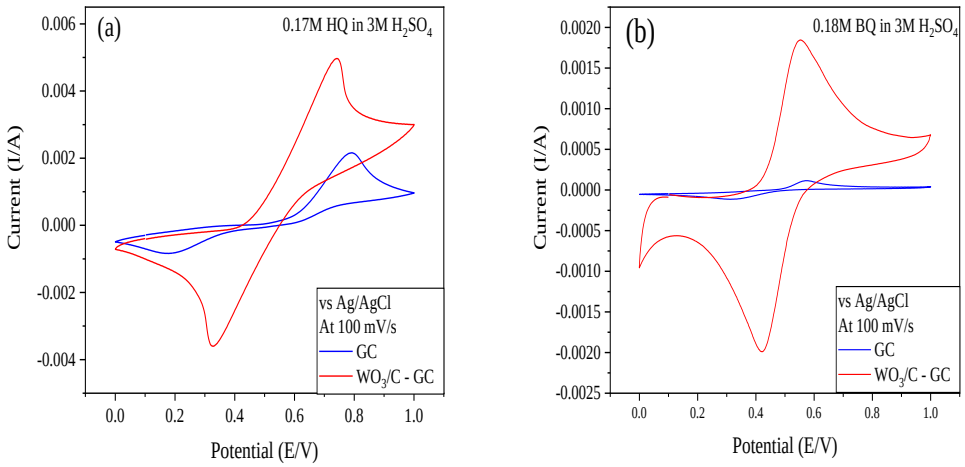

Figure 5.6. Cyclic voltammograms using GC and WO_3/C electrocatalyst in (a) Hydroquinone (0.17M in 3M H_2SO_4) solution (b) Benzoquinone (0.18M in 3M H_2SO_4) Solution

Table 5.2 Parameter analysis of voltammograms

Electrode	**I_{pa}(mA)**	**I_{pc}(mA)**	**E_{pa}(V)**	**E_{pc}(V)**	**E_{pa}- E_{pc} (V)**	**I_{pa}/ I_{pc}**
GC	2.158	0.785	0.791	0.163	0.628	2.74
WO_3/C-GC	4.96	3.591	0.74	0.324	0.416	1.38

After assessing the performance of the developed WO_3/C catalyst on GC by CV, similar procedure was adopted to test the real electrode WO_3/C-CP in 0.17M in 3M H_2SO_4 and 0.18M in 3M H_2SO_4 electrolyte. The voltammograms of both half cells of HQ-BQ RFB employing WO_3/C-CP, TiO_2@CNP-CP, and CP are compared and shown in Figure 5.7a and Figure 5.7b.

The WO_3/C electrocatalyst is giving relatively enhanced peak current values in both the half cells as shown in Table 5.3.

Table 5.3 Peak currents of the electrodes

Half-cell→ Electrode	**Positive half cell**		**Negative half cell**	
	Ipa (A)	Ipc (A)	Ipa (A)	Ipc (A)
CP	0.03	-0.02	0.076	-0.05
TiO_2@CNP-CP	0.1	-0.12	0.11	-0.059
WO_3/C-CP	0.158	-0.17	0.147	-0.07

This can be attributed to higher catalytic activity with enhanced active surface area of WO_3/C-CP. Further, it is also confirmed by calculating the ECSA by procedure explained in the section 3.4. The CV tests at different scan rates were carried out by using WO_3/C-CP, TiO_2@CNP-CP, and CP electrodes in both half-cells of HQ-BQ RFB. The current values were read in non-faradaic region at 0.2 V, plotted against the scan rate and obtained the values of C_{dl} as shown Figure 5.8.

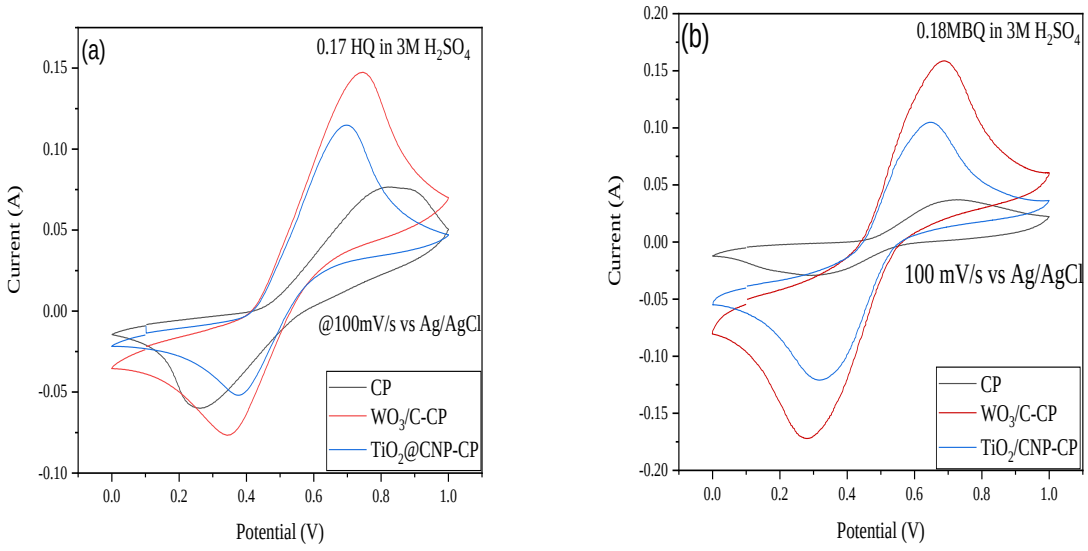

Figure 5.7 Cyclic voltammograms of CP, TiO_2@CNP-CP and WO_3/C-CP in (a) HQ electrolyte system (b) BQ electrolyte system

The specific capacitance (Cs) was calculated using standard carbon paper electrode in 0.17M HQ in 3M H_2SO_4 and 0.18M BQ in 3M H_2SO_4 are found out to be 0.025 F/cm^2 and 0.018 F/cm^2

respectively. The calculated ECSA, TOF and number of active sites were estimated using the cyclic voltammograms corresponding to WO_3/C-CP, TiO_2@CNP and CP are tabulated in Table 5.4.

Table 5.4. Summary of ECSA and TOF of electrodes in both the half cells of HQ-BQ RFB

Half-cell→	**Positive half cell**			**Negative half cell**		
Electrode	ECSA (cm^2)	Active sites (mol)	TOF (s^{-1})	ECSA (cm^2)	Active sites (mol)	TOF (s^{-1})
CP	1	1.1×10^{-6}	0.17	1.14	$1.7*10^{-6}$	0.032
TiO_2@CNP-CP	8.33	2.7×10^{-6}	0.18	2.25	$1.8*10^{-6}$	0.066
WO_3/C-CP	10	4.3×10^{-6}	0.19	4.8	$2.6*10^{-6}$	0.079

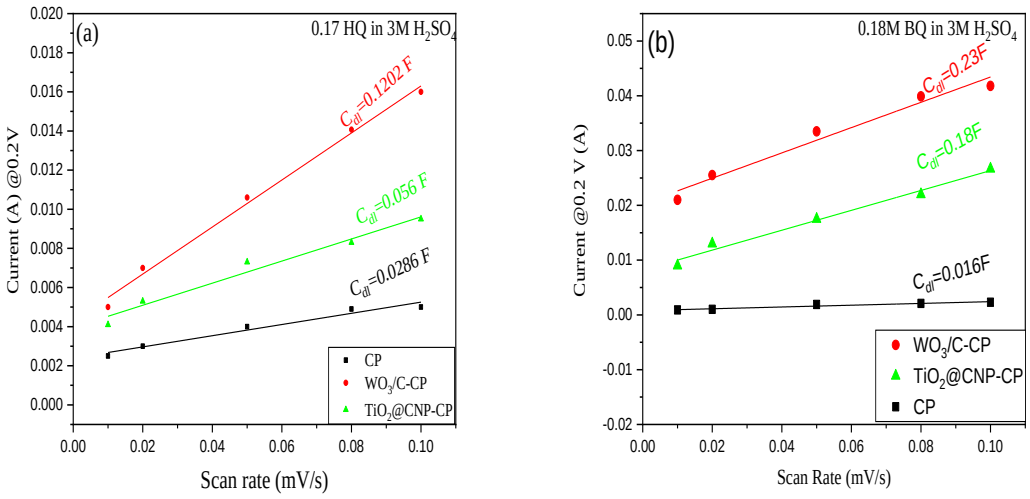

Figure 5.8 Electrochemical Double layer capacitance (C_{dl}) of TiO_2@CNP-CP and WO_3/C-CP and CP in (a) HQ electrolyte system (b) BQ electrolyte system

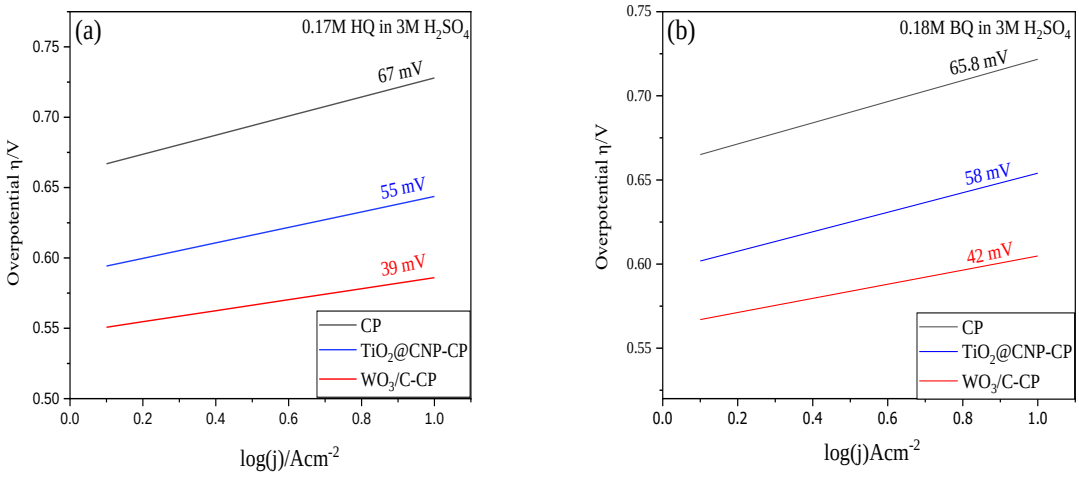

Figure 5.9 Tafel plots of TiO_2@CNP-CP and WO_3/C-CP and CP in (a) HQ electrolyte system (b) BQ electrolyte system

ECSA of WO_3/C-CP and TiO_2@CNP-CP in positive half-cell of HQ-BQ RFB are 10 cm^2 and 8.33 cm^2 respectively while in negative half-cell of HQ-BQ RFB are 4.8 cm^2 and 2.25 cm^2. Which implies that the WO_3/C-CP provides more active sites for the reactions to take place in the battery system. The calculated number of active sites of WO_3/C-CP in positive half-cell and in negative half-cell of HQ-BQ RFB are 4.3×10^{-6} mol and 2.6×10^{-6} mol respectively. The corresponding TOF of WO_3/C-CP in positive half-cell and in negative half-cell of HQ-BQ RFB are 0.19 s^{-1} and 0.079 s^{-1} respectively. It is observed that these values are higher than that of CP, TiO_2@CNP-CP and possesses the improved catalytic activity of WO_3/C electrocatalyst.

The data represented in Figure 5.7 was further subjected to Tafel analysis and the tafel plots are shown in Figure 5.9. The Tafel slope for WO_3/C-CP electrode is 39.1 mV in negative half-cell and 42 mV in positive half-cell which are significantly lower than slopes of TiO_2@CNP (55mV in negative half-cell and 58mV in positive half-cell) and CP (67.8 mV in negative half-cell and 65.8 mV in positive half-cell). It indicates that the reaction kinetics for the HQ and BQ system is increased significantly using WO_3/C electrocatalyst.

5.3 Single-cell charge-discharge

The charge-discharge test of single cell HQ-BQ RFB was carried out at a constant current density of 10 mA.cm^{-2} by employing WO_3/C-CP, TiO_2@CNP-CP, and CP electrodes.The performance of the cell is compared over 50 charge-discharge cycles and shown in Figure 5.10.

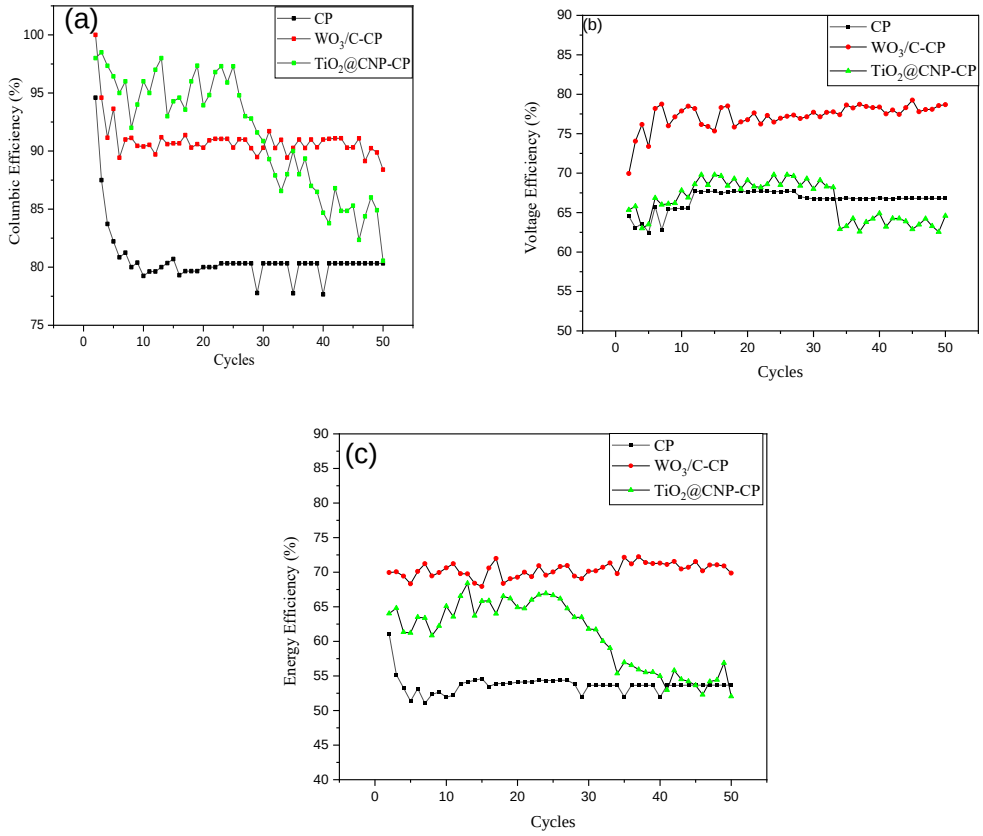

Figure 5.10**. S**ingle cell performance of WO_3/C-CP, TiO_2@CNP-CP, and CP in HQ-BQ RFB (a) CE, (b) VE, (c) EE

In the initial stages of the charge-discharge cycles, it becomes evident in figure 5.10(a) that the coulombic efficiency (CE) is gradually declining over subsequent cycles until reaching a stable state upto few cycles (<10). Following this stabilization period, the CE of the HQ-BQ redox flow battery utilizing WO_3/C-CP consistently hovers around 90%, indicating robust and reliable performance. Concurrently, the voltage efficiency (VE) maintains an average of approximately 75%, while the energy efficiency (EE) remains steadfast at around 70% throughout the duration

of over 50 charge-discharge cycles. Conversely, the CE and VE profiles of the HQ-BQ RFB with TiO_2@CNP-CP exhibit fluctuations and a downward trend over time.

This inconsistency is mirrored in the performance of the carbon paper (CP) electrodes, which display lower and irregular CE and VE values. Notably, the energy efficiency of the HQ-BQ RFB employing CP and TiO2@CNP electrodes dwindles to 55% and 60%, respectively. The GCD cycles are shown in figure 5.11. These observations suggest that both CP and TiO_2@CNP electrodes may not be optimally suited for this application. However, in stark contrast, the WO_3/C-CP electrodes demonstrate remarkable resilience and consistently outperform their counterparts.

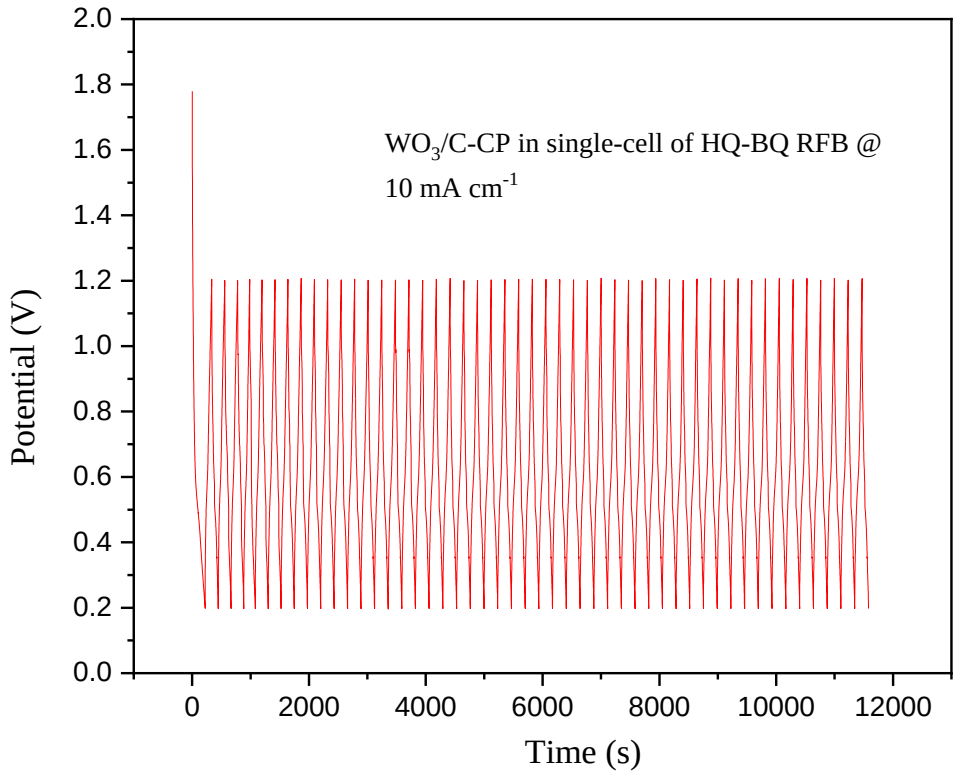

Figure 5.11**. S**ingle cell GCD cycles of WO_3/C-CP in HQ-BQ RFB

They exhibit robust performance and yield improved outcomes in the HQ-BQ RFB, with CE, VE, and EE values maintaining stability and efficiency levels throughout the experimental

duration. These findings underscore the superior suitability and enhanced performance of WO_3/C-CP electrodes in HQ-BQ RFB applications. These insights contribute to advancing the understanding of electrode-material dynamics in redox flow batteries, facilitating informed decisions for optimizing battery performance and enhancing overall efficiency in energy storage applications.

5.4 Conclusion

The highly active nano-WO_3/C electrocatalyst was successfully developed which can enhance electrochemical activity and electro kinetic reversibility of half-cell reactions of the HQ-BQ RFB. The WO_3 doping in activated carbon has improved the reaction kinetics by forming the adsorption bonds with the reactant active species. The solubilities of HQ and BQ in 3M H_2SO_4 were optimized as 0.17 mol/l and 0.18 mol/l respectively and these concentrations were used for CV and single cell charge-discharge tests. The increased surface roughness was observed for electrocatalyst coated CP under FESEM indicating the more available active sites for the reaction. The electrocatalyst was proved to be crystalline from XRD which helps in enhancing electrochemical activity. The characteristic functional bonds of WO_3/C were identified by FTIR. The CV curves of WO_3/C-CP showed higher peak current values with lower peak separation. The results are compared with that of previously synthesized TiO_2@CNP-CP which is explained in chapter 4. The Tafel slope of WO_3/C electrocatalyst is lower than the TiO_2@CNP-CP comparatively in both half cells of HQ-BQ RFB. The Tafel slopes of WO_3/C electrocatalyst in positive and negative half-cell of HQ-BQ RFB are 42 mV and 39.1 mV. These lower values indicate the enhanced reaction kinetics. ECSA of WO_3/C-CP in positive and negative half-cell of HQ-BQ RFB are 10 cm^2 and 4.8 cm^2 respectively which are relatively larger than that of TiO_2@CNP-CP (6.77 cm^2 in positive half-cell and 2.25 cm^2 in negative half-cell). The number of active sites and TOF values are also higher for WO_3/C in both the half cells of BQ-BQ RFB among all the three electrodes. The CE, VE, and EE of HQ-BQ flow

battery using, CP were around 80%, 67% and 53% respectively and TiO_2@CNP-CP were around 92%, 65% and 60% respectively. While the values of CE, VE, and EE of HQ-BQ flow battery using synthesized WO_3/C electrocatalyst were around 90%, 75%, and 70% respectively, which were much higher than those of HQ-BQ RFBs using CP and TiO_2@CNP-CP.

References

Guéry, C., Choquet, C., Dujeancourt, F., Tarascon, J. M., & Lassègues, J. C. (1997). Infrared and X-ray studies of hydrogen intercalation in different tungsten trioxides and tungsten trioxide hydrates. Journal of Solid State Electrochemistry, 1(3), 199–207. https://doi.org/10.1007/s100080050049

Hoffmann, P., Galindo, H., Zambrano, G., Rincón, C., & Prieto, P. (2003). FTIR studies of tungsten carbide in bulk material and thin film samples. Materials Characterization, 50(4), 255–259.
https://doi.org/10.1016/S1044-5803(03)00100-1

Jeong, S., Kim, S., & Kwon, Y. (2013). Performance enhancement in vanadium redox flow battery using platinum-based electrocatalyst synthesized by polyol process. Electrochimica Acta, 114, 439–447.
https://doi.org/10.1016/j.electacta.2013.10.011

Jiang, W.-J., Niu, S., Tang, T., Zhang, Q.-H., Liu, X.-Z., Zhang, Y., Chen, Y.-Y., Li, J.-H., Gu, L., Wan, L.-J., & Hu, J.-S. (2017). Crystallinity-Modulated Electrocatalytic Activity of a Nickel(II) Borate Thin Layer on Ni3B for Efficient Water Oxidation. Angewandte Chemie, 129(23), 6672–6677.
https://doi.org/10.1002/ange.201703183

Jothivenkatachalam, K., Prabhu, S., Nithya, A., & Jeganathan, K. (2014). Facile synthesis of WO3 with reduced particle size on zeolite and enhanced photocatalytic activity. RSC Advances, 4(41), 21221–21229.
https://doi.org/10.1039/C4RA01376J

Kushner, D. I., Crothers, A. R., Kusoglu, A., & Weber, A. Z. (2020). Transport phenomena in flow battery ion-conducting membranes. Current Opinion in Electrochemistry, 21, 132–139. https://doi.org/10.1016/j.coelec.2020.01.010

Waring, J. (1966). Phase equilibria as related to crystal structure in the system niobium pentoxide-tungsten trioxide. l(4).
DOI: 10.6028/jres.070A.025

CHAPTER 6

CONCLUSION

CHAPTER 6

CONCLUSION

The electrocatalysts of TiO_2@CNP and WO_3/C were successfully synthesized for H_2 -BQ RFB and HQ-BQ RFB using the ultrasonic dispersion method. The TiO_2@CNP was developed for the positive (anodic) half-cell in the H_2-BQ RFB and layered onto carbon paper using the drop-casting technique. The surface of the coated carbon paper was examined by SEM, revealing the presence of textured fibers on the surface. Additionally, FTIR analysis confirmed the existence of functional bonds associated with the interaction between TiO_2 and carbon. XRD analysis established a partially crystalline TiO_2@CNP structure comprising anatase and rutile phases. The composition of (TiO_2+C: Nafion) in TiO_2@CNP was optimized using CV test. Further, the electrochemical performance of TiO_2@CNP-CP was assessed in the positive half-cell of H_2-BQ RFB. In CV, TiO_2@CNP-CP demonstrated higher peak current densities of 5.4 $mAcm^{-2}$ and minimal peak separation compared to CNP-CP. The Tafel slopes of CP, CNP-CP, and TiO_2@CNP-CP are 121.8 mV, 54 mV, and 18 mV, respectively.

The lower slope of the TiO_2@CNP-CP suggests enhanced reaction kinetics. The determined ECSAs of TiO_2@CNP-CP, CNP-CP, and CP are 8.32 cm^2, 6.8 cm^2 and 4.4 cm^2 respectively. The TiO_2@CNP-CP electrode has a higher ECSA and a greater number of active sites than CP and CNP-CP electrodes, which provide higher catalytic activity. The catalyst's performance was tested in H_2-BQ RFB positive half-cell and subjected to 50 cycles of charge-discharge at 1.6 mA cm^{-2} current density. The cell achieved an energy efficiency of 73%, which is significantly higher than that of pristine carbon paper, establishing its suitability for application within the H_2-BQ RFB system.

A highly active nano WO_3/C electrocatalyst was developed for HQ-BQ RFB, and a comparison study was made with the CP and TiO_2@CNP-CP. The increased surface roughness was observed for electrocatalyst-coated CP under FESEM, indicating the more available active sites for the reaction. The electrocatalyst was proved to be partially crystalline from XRD, which helps in enhancing electrochemical activity. The characteristic functional bonds of WO_3/C were identified by FTIR. Further, the solubilities of the active materials in the supporting electrolyte have been optimized at 0.17M HQ in 3 M H_2SO_4 and 0.18M BQ in 3 M H_2SO_4. The CV curves of WO_3/C-CP showed higher peak current values with lower peak separation as compared to CP and TiO_2@CNP-CP. The WO_3 doping in activated carbon has improved the reaction kinetics by forming the adsorption bonds with the reactant active species. The Tafel slope of WO_3/C electrocatalyst is lower than the TiO_2@CNP-CP comparatively in both half cells of HQ-BQ RFB. The Tafel slopes of WO_3/C electrocatalyst in positive and negative half-cells of HQ-BQ RFB are 42 mV and 39.1 mV. These lower values indicate enhanced reaction kinetics. ECSA of WO_3/C-CP in positive and negative half-cells of HQ-BQ RFB is 10 cm^2 and 4.8 cm^2, respectively, which are relatively larger than that of TiO_2@CNP-CP (6.77 cm^2 in positive half-cell and 2.25 cm^2 in negative half-cell). The number of active sites and TOF values are also higher for WO_3/C in both the half cells of BQ-BQ RFB among all three electrodes. The CE,

VE, and EE of HQ-BQ flow battery using CP were around 80%, 67%, and 53%, respectively, and TiO_2@CNP-CP were around 92%, 65%, and 60%, respectively. While the values of CE, VE, and EE of HQ-BQ flow battery using synthesized WO_3/C electrocatalyst were around 90%, 75%, and 70% respectively, which were much higher than those of HQ-BQ RFBs using CP and TiO_2@CNP-CP. The developed non-noble WO_3/C and TiO_2@CNP electrocatalysts proved their suitability in proposed H_2-BQ RFB and HQ-BQ RFB systems by providing higher active sites and reaction kinetics.

Scope for future work

In the pursuit of advancing energy storage solutions and sustainable technology, this research has successfully developed and characterized two promising electrocatalysts for quinone-based redox flow batteries (RFBs) with optimized electrolyte composition. While the current work has laid a solid foundation, the journey toward practical and scalable energy storage is multifaceted, opening doors to several exciting avenues for future exploration. Following are the potential future extensions of the present work

- The effect of physical parameters like flow rates, temperature, and concentrations can be varied and optimized for the proposed RFB systems.
- Extended cycling tests can be performed to simulate real-world usage by assessing electrocatalysts for the optimized composition of electrolytes in HQ-BQ RFB.
- Integrating renewable electricity for charge-discharge of lab-scale quinone-based RFB can aid in technology validation.
- Development of mathematical models and simulations tailored explicitly to the RFB lab-scale experiments. These models can assist in understanding the fundamental processes occurring within the system and predicting behavior under varying conditions.

- Comparative studies can be conducted with other lab-scale RFBs using the developed electrocatalysts. This thesis work can help benchmark the technology's performance and identify improvement areas.
- Exploration of different additives and concentrations to enhance the electrochemical characteristics and stability of HQ and BQ electrolytes.

List of articles published in international journals

1. **Irshad U. Khan,** Murali Mohan Seepana, K.S.Rajmohan, Jay Pandey "Electrochemical activity of tungsten oxide doped carbon (WO_3/C) catalyst for hydroquinone/benzoquinone redox flow battery." Materials Letters. ***https://doi.org/10.1016/j.matlet.2023.134355*** **(SCI: Elsevier),** Impact factor: 3.0

2. **Irshad U. Khan,** K.S.Rajmohan, Murali Mohan Seepana, "Synthesis and Electrocatalytic Performance of TiO_2 Supported on Carbon Nanoparticles Towards Positive Half-Cell Reaction of Hydrogen-1,4p-benzoquinone Flow-Battery." Journal of The Electrochemical Society, ***doi 10.1149/1945-7111/ace002*** (SCI), Impact factor: 3.9

List of international conferences

1. **Irshad U. Khan,** K.S. Rajmohan and Murali Mohan Seepana, "Carbon-based Electrocatalyst for Quinone based Redox Flow Battery", CHEMCON 2021, 26-30 December 2021, Bhubaneshwar, INDIA.

2. **Irshad U. Khan,** Tanmay Paul, Murali Mohan Seepana, "Copper Oxide Doped Carbon Catalyst for Anodic Half-Cell of Vanadium Redox Flow Battery (VRFB)", ICCME 2023: XVII, 10-11 July 2023, Toronto, CANADA.

BIOGRAPHY

Mr. Irshad comes from Lanji, Madhya Pradesh, and is a dedicated researcher with a strong background in chemical engineering. His academic journey commenced at Laxminarayan Institute of Technology, Nagpur, where he earned his Bachelor's degree in Chemical Engineering (B.Tech) in June 2016. Building on this foundation, he pursued advanced studies, obtaining a Master's degree in Chemical Engineering (M.Tech) from the prestigious National Institute of Technology, Warangal, completing his degree in June 2019. In August 2019, Mr. Irshad started his Ph.D. at National Institute of Technology, Warangal. Here, he actively contributed to the Indo-UK SPARC project, focusing on the development of non-noble electrocatalysts for organic redox flow batteries. His research work has a specific emphasis on the synthesis and characterization of metal oxide-based electrocatalysts for quinone-based organic redox flow batteries. Notable achievements include the development of TiO_2@CNP and WO_3/C electrocatalysts tailored for redox flow battery applications. Currently, Mr. Irshad is submitting his Ph.D. work. His Ph.D. thesis title is "Development of Non-Noble Electrocatalysts for Quinone-Based Organic Redox Flow Batteries." His passion for energy storage systems as sustainable solutions is evident in both his academic pursuits and practical contributions to the field. In addition to his academic endeavors, Mr. Irshad has actively disseminated his research findings. He has published articles in reputable scientific journals and presented his research at international conferences. His commitment to advancing knowledge in the field of energy storage underscores his dedication to sustainable solutions for the future.